REPORT DOCUMENTATION PAGE	Form Approved OMB No. 0704-0188

1. AGENCY USE ONLY *(Leave blank)*	2. REPORT DATE	3. REPORT TYPE AND DATES COVERED
	4 August 1998	

4. TITLE AND SUBTITLE
AN ENVESTIGATION INTO THE PASSIVE DETECTION OF POINT TARGETS USING FM BROADCASTS OR WHITE NOISE

5. FUNDING NUMBERS

6. AUTHOR(S)
Chadwick D. Lindstrom

7. PERFORMING ORGANIZATION NAME(S) AND ADDRESS(ES)
University of Washington

8. PERFORMING ORGANIZATION REPORT NUMBER
98-038

9. SPONSORING/MONITORING AGENCY NAME(S) AND ADDRESS(ES)
THE DEPARTMENT OF THE AIR FORCE
AFIT/CIA, BLDG 125
2950 P STREET
WPAFB OH 45433

10. SPONSORING/MONITORING AGENCY REPORT NUMBER

11. SUPPLEMENTARY NOTES

12a. DISTRIBUTION AVAILABILITY STATEMENT
Unlimited distribution
In Accordance With AFI 35-205/AFIT Sup 1

12b. DISTRIBUTION CODE

13. ABSTRACT *(Maximum 200 words)*

14. SUBJECT TERMS	15. NUMBER OF PAGES
	82
	16. PRICE CODE

17. SECURITY CLASSIFICATION OF REPORT	18. SECURITY CLASSIFICATION OF THIS PAGE	19. SECURITY CLASSIFICATION OF ABSTRACT	20. LIMITATION OF ABSTRACT

Standard Form 298 (Rev. 2-89) (EG)
Prescribed by ANSI Std. 239.18
Designed using Perform Pro, WHS/DIOR, Oct 94

AN INVESTIGATION INTO THE PASSIVE DETECTION OF POINT TARGETS USING FM BROADCASTS OR WHITE NOISE

by

Chadwick D. Lindstrom

A thesis submitted in partial fulfillment of the requirements for the degree of

Master of Science in Electrical Engineering

University of Washington

1997

Approved by _____
Chairperson of Supervisory Committee

_____

Program Authorized
to Offer Degree _____

Date _____

Master's Thesis

In presenting this thesis in partial fulfillment of the requirements for a Master's degree at the University of Washington, I agree that the Library shall make its copies freely available for inspection. I further agree that extensive copying of this thesis is allowable only for scholarly purposes, consistent with "fair use" as prescribed in the U.S. Copyright Law. Any other reproduction for any purposes or by any means shall not be allowed without my written permission.

Signature Chris D. Lott

Date 21 Oct 97

TABLE OF CONTENTS

LIST OF FIGURES

LIST OF TABLES

ACKNOWLEDGMENTS

I wish to thank John Sahr, my thesis advisor, for encouragement and insight during this research project. Also, I would like to thank Frank Lind for providing the data sets that were used throughout this thesis, and for providing a practical perspective on radar receiver operation.

INTRODUCTION

Over the past three years, researchers at the University of Washington have been developing a multistatic radar system that uses commercial FM radio broadcasts to detect plasma waves in the ionosphere. This research has shown that the short autocorrelation times of FM broadcasts make it possible to achieve good range and doppler resolution despite the continuos operation of the transmitter However, because of the great distances of ionospheric targets (>600 km) most research has focused on a multistatic system consisting of a reference receiver and another receiver isolated from the direct broadcast signal by the Cascade Mountains. Although some research was done on a bistatic system, it was quickly seen that the clutter limited dynamic range would make the observation of plasma waves very difficult if not impossible. This analysis though did not rule out the detection of aircraft at distances close to the receiver-transmitter baseline. In fact, the first detection using FM broadcasts was that of a bistatic detection of an aircraft displaced 1.5 km from the baseline [1].

The primary problem with the detection of aircraft with the bistatic radar is discriminating the scattered signal(s) against the strong direct broadcast. This is similar to the detection of weak signals against strong interfering white noise sources as encountered in sonar and radar environments with strong ECM (electronic countermeasures). The optimal solution is known to be matched filtering combined with spatial filtering technique such as adaptive beamforming [2]. However, because the signal we are seeking to identify is not known before reception it is impossible to use the traditional matched filtering technique. Instead, we compute the self-ambiguity function of the signal. This is still optimal if the signal itself is white noise, but it requires that the scattered signal compete with the clutter of the direct signal. A performance analysis of this technique is done for the case of white noise which is then phenomenologically extended to FM radio

broadcasts. The key results of this analysis are that detection of aircraft will probably not be possible at FM broadcast bandwidths. However, the theory developed for white noise processes shows that a spread spectrum radar which uses 10 - 20 Mhz of bandwidth could be developed with a range radius of 4 - 5 km from the receiver. Although not interesting by itself, a network of the receivers could be formed whose presence would be impossible to detect since they would be completely passive. Also, because the spectral density of the transmitted signal would be close to the noise floor, it would even be difficult to determine the radar's presence. This would allow an active transmitter to be used.

CHAPTER 1: SYSTEM OVERVIEW AND REQUIREMENTS

As with any system analysis problem, before we begin the detailed analysis of the capabilities of the radar it is necessary to ensure that the reader understand at the broad system(s) level the radar operation. A radar is a system which generally consists of a transmitter, receiver, antenna(s), and either analog or digital equipment which implements a signal processing routine on the raw receiver data [3]. The purpose of the signal processing routine is to use the principles of electromagnetic theory along with that of statistics to detect and determine characteristics such as range, direction, or velocity of a target(s).

The major differences between a system which uses commercial FM radio broadcasts and that of a conventional radar come from the operator not controlling the transmitted waveform and from the separation of the receiver and transmitter. The inability to control the waveform requires that the signal must be modeled in order to analyze its performance. We will be modeling the transmitted signal as white gaussian noise which is primarily done for analytical convenience, but we will also show how the model can be extended to colored gaussian noise which more accurately describes the FM broadcast. The separation of the receiver and transmitter means that the geometry and location of the receivers will be very important. It also has the effect that the receiver topology can be simplified to direct conversion.

1.1 RECEIVER TOPOLOGY

The direct conversion receiver can be used in this radar since there is no transmitter sharing the same antenna as the receiver. Hence, the traditional interference problem which requires that the signal first be mixed with an intermediate frequency is not required. Thus, the receiver topology for this radar is given by figure 1.1 [3]:

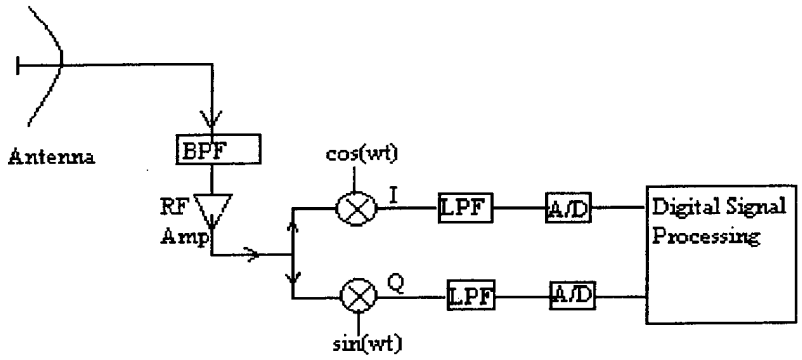

Figure 1.1: Direct Conversion Receiver

1.2 BASIC SIGNAL PROCESSING ALGORITHM

The optimal linear detection algorithm in radar and also for other applications which must detect signals in noise is matched filtering [2]. In the time domain, because the impulse response of the matched filter is the time reversed conjugate of the signal, matched filtering is equivalent to correlating the received signal with the signal that was transmitted. This intuitively makes sense because we would expect the algorithm to compare the transmitted signal to what was transmitted. The matched filtering allows us to quantitatively determine the degree of correlation between the signal that was transmitted and what has been received and it does this in the optimal sense of maximizing the SNR (signal to noise ratio).

The bistatic FM radar uses just one receiver which records a vector sum of both the direct and the scattered signal as shown in figure 1.3. To be able to record both signals simultaneously requires sufficient dynamic range. This is primarily determined by the number of bits of the analog to digital converter. The matched filtering is implemented by correlating the received signal with itself. There will be a large spike in the ambiguity function at zero delay and doppler shift because the signal perfectly matches itself.

Targets must now compete with the noise plus the clutter of the direct signal. Characterizing the clutter of the direct signal is the main problem that must be understood to determine the sensitivity of the radar.

1.3 RECEIVER GEOMETRY

The location of the receivers is important in understanding the operation of the radar. Several options are open to the designer each of which offers its own advantages and problems.

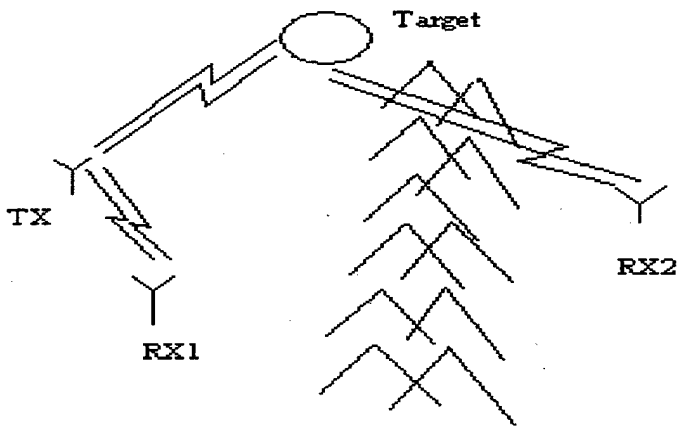

Figure 1.2: Multistatic Receiver Geometry. The direct signal is received at RX1 and correlated with the scattered signal received at RX2. The direct signal is blocked by the Cascade Mountains which allows RX2 to receive only the scattered signal.

The first design is given in figure 1.2. This is the multistatic radar which is examined extensively in Paul Hall's thesis [4]. It has the advantage that the mountain range blocks the direct signal to the second receiver. This alleviates the dynamic range and some of the clutter problems which are present in the bistatic geometry. Unfortunately, this method of implementation requires suitable geographic features which limits its use to a few select regions of the world. It also has the problem that a relatively high speed data link be

established between the two receivers. Finally, this geometry has been extensively investigated by researchers at the University of Washington.

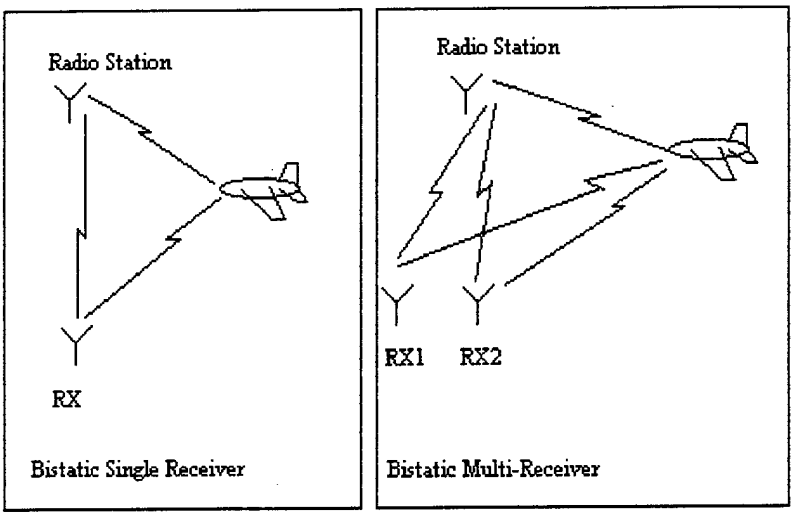

Figure 1.3: Illustration of Bistatic Geometry. In both cases, the receivers must receive a vector sum of the direct and scattered signals.

Figure 1.3 shows the single receiver bistatic radar. It requires the least amount of hardware with only a single receiver. However, the simplicity in hardware components is offset by the requirement to distinguish targets against the strong direct signal whose self clutter will obscure targets.

This problem may be partially dealt with by using two directional antennas one pointed at the receiver and the other in the direction of the target. This can also be be done by using two or more closely spaced receivers (within several wavelengths of each other). It is then possible to use the phase differences due to the difference in the path lengths to cancel the direct signal which can be implemented through the spatial filtering technique called adaptive beamforming. Of course this requires two or more receivers to be built, as well as an increase in the computation burden which are the systems main drawbacks.

be built, as well as an increase in the computation burden which are the systems main drawbacks.

1.4 SENSITIVITY REQUIREMENTS

The sensitivity requirements can be determined from the bistatic radar equation. This is given by (ignoring polarization or impedance mismatch) [5] :

$$P_{rs} = \frac{\lambda^2 G_t(\hat{i}) G_r(-\hat{o}) \sigma_{bi}(\hat{o},\hat{i})}{(4\pi)^3 R_1^2 R_2^2} P_t \tag{1.1}$$

where P_r, P_t are the power at the receiver and transmitter respectively. The two gain factors, $G_t(\hat{i})$ - transmitter antenna gain and $G_r(\hat{o})$ - receiver antenna gain, are dependent upon direction patterns which is the reason for the vector arguments. The bistatic cross section, $\sigma_{bi}(\hat{o},\hat{i})$ is the parameter determined by the target and is also dependent upon direction. The factor λ^2 is the wavelength of the carrier frequency and results from the receiver cross section. The final two factors, R_1 and R_2 are defined in the figure 1.4. Similarly, the received power of the direct signal can be written as:

$$P_r = \frac{\lambda^2 G_t(\hat{i}') G_r(-\hat{i}')}{(4\pi)^2 L^2} P_t \tag{1.2}$$

where the prime indicates the directions will often be different from the scattered signal.

The two quantities which are pertinent to the problem of interest is the ratio of 1.1 to 1.2, and the ratio of 1.1 to noise power. First, we write the ratio of the received power of the scattered signal relative to the direct signal (1.1 to 1.2):

$$\frac{P_{rs}}{P_r} = \alpha^2 = \frac{\rho \sigma_{bi}(\hat{i},\hat{o}) L^2}{(4\pi) R_1^2 R_2^2} \qquad \rho = \frac{G_t(\hat{i}) G_r(\hat{o})}{G_t(\hat{i}') G_r(\hat{o}')} \tag{1.3}$$

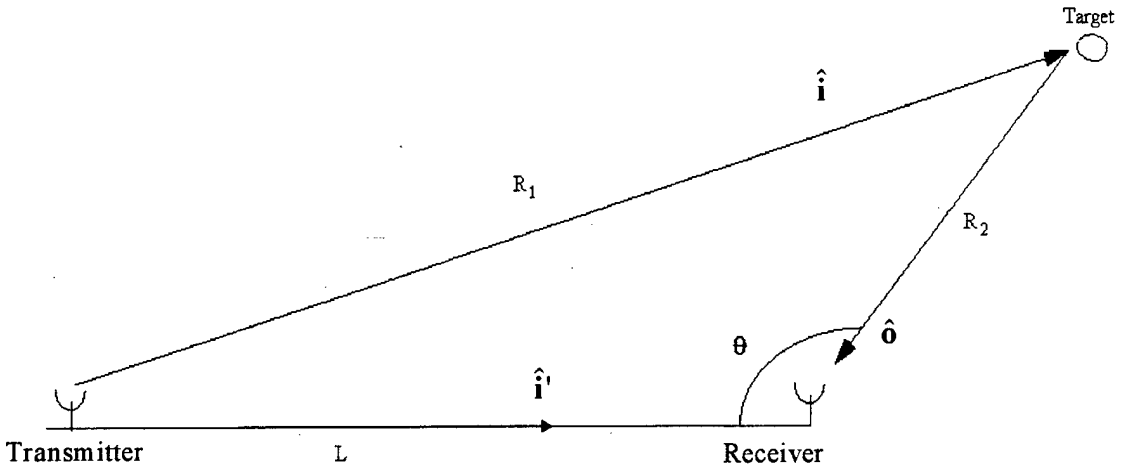

Figure 1.4: The bistatic triangle.

We will call this quantity the scattered to direct ratio (SDR). It will often be the case that we will be operating with $P_r >> N$ where N is the noise power. Thus, it is useful to determine the performance of the system for a minimum SDR and specific values of L, ρ, and $\sigma_{bi}(\hat{o},\hat{i})$. The requirements on R_1 and R_2 are then that they satisfy the law of cosines with L being the third side of the triangle as shown in figure 1.3, and that they satisfy equation 1.3 for the given values. It is then easy to show R_2 must obey the following quartic equation with θ being defined as indicated in figure 1.4:

$$R_2^4 - 2LR_2^3\cos(\theta) + L^2R_2^2 - \frac{\sigma_{bi}(\hat{i},\hat{o})L^2}{(4\pi)\alpha_{\min}^2} = 0 \qquad (1.4)$$

Notice that for small R_2 that 1.4 reduces to the familiar equation of a circle in polar coordinates. This is one possible equation that can be used to describe the Ovals of

Cassini that result, and other solutions that use a different origin or coordinate system exist [2]. This equation although difficult to solve analytically can easily be plotted with

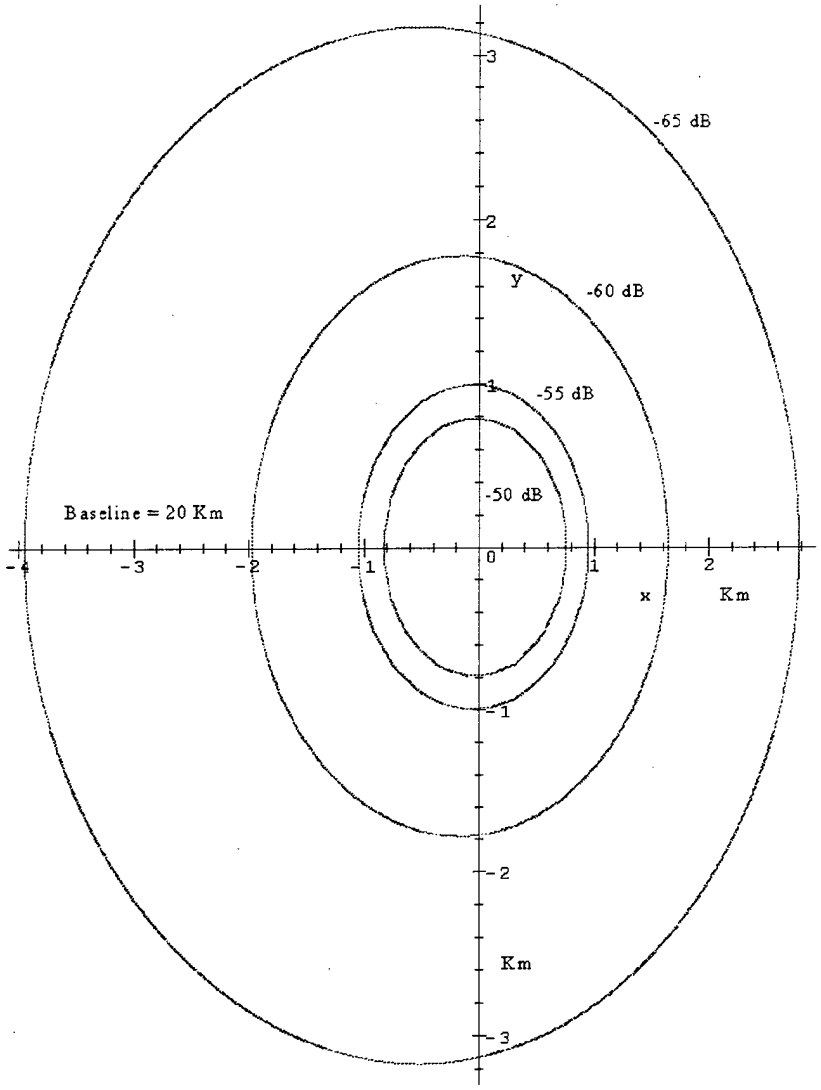

Figure 1.5: Plot of ovals of Cassini about the receiver with L = 20 Km, $\sigma_{bi}(\hat{o},\hat{i}) = 40$ m^2, $\rho = 1$, and $\alpha^2_{\min}$ as given on the curves.

the implicit plot function of Maple. The result for various values of α^2_{min} is shown in figure 1.5. This indicates that we must be capable of detecting scatter -55 dB below the transmitter signal to be able to detect a target with a cross section the size of an

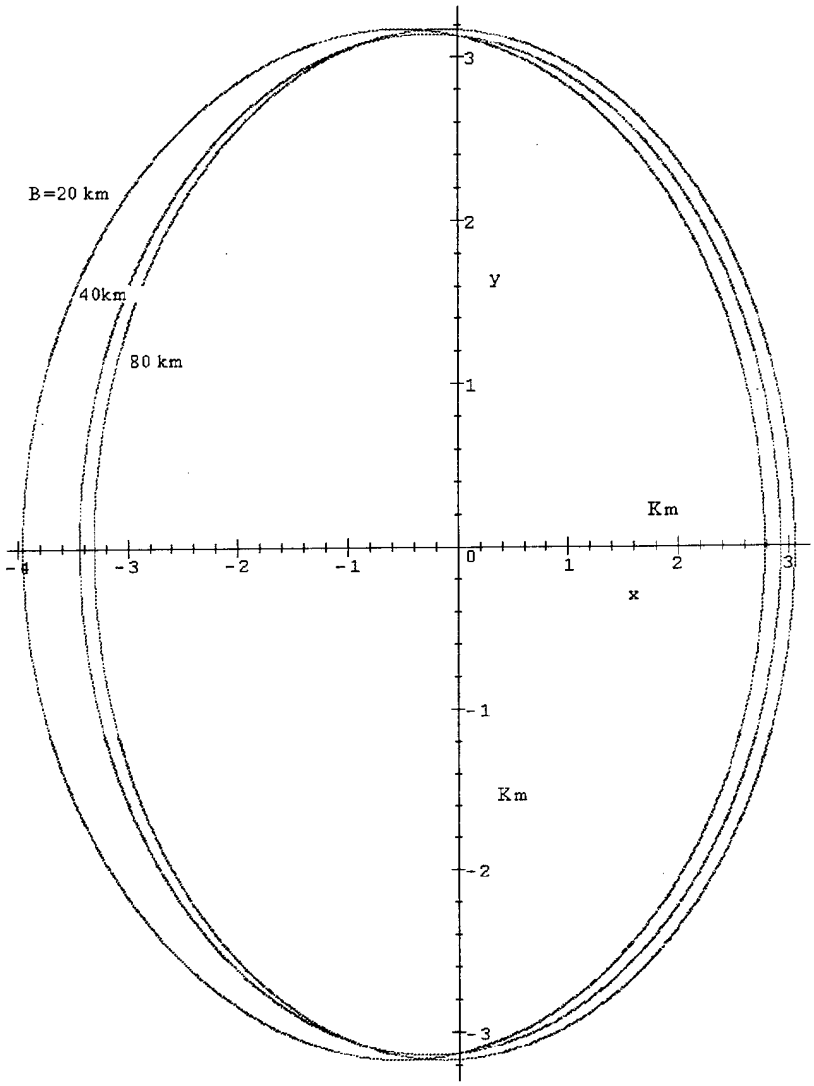

Figure 1.6: Ovals of Cassini for indicated baseline lengths and α^2_{min} = -65 dB, ρ=1 and $\sigma_{bi}(\hat{o},\hat{i}) = 40$ m^2.

airliner, 40 m^2, at 1 km from the receiver without directional antennas. However, a similar mirror image of the ovals occur about the transmitter which means it is possible to detect a target 21 km away. It is also important to see as shown in figure 1.6 that the ovals described by equation 1.4 are quite close for varied baseline lengths. The reason for this is that both the scattered signal and the direct signal depend upon the baseline length. Hence, when the power ratio is taken the change due to the baseline length changing is typically small.

Next, we use the model that the noise is white and hence its power can be written as [5]:

$$N = k_B T f_B \tag{1.4}$$

$k_B = 1.38 \times 10^{-23}$ J/K is Boltzman's constant, T is the noise temperature of the receiver plus the cosmic background radiation, and f_B is the bandwidth of the receiver. This means that the ratio of the scattered signal to the noise (SNR) is given by:

$$\frac{P_{rs}}{N} = \frac{\lambda^2 G_t(\hat{i}) G_r(\hat{o}) \sigma_{bi}(\hat{i},\hat{o}) P_t}{(4\pi)^3 R_1^2 R_2^2 k_B T f_B} \tag{1.5}$$

Normally T is taken close to the effective cosmic temperature which can obtain a maximum of 10,000 K, however, in this case it was found the measured noise power was closer to -60 dBm because of the loud radio environment in the Seattle area due to factors such as FM sidebands [1]. This means that T should be taken as 2.89×10^8 K. However, this still only results in an SNR of about -25.5 dB for a baseline length of 80 km and 100 kW transmitter power which is much higher than the corresponding SDR. Indeed, if we can handle the SDR then it will be possible to easily deal with the noise at almost all baseline lengths of interest.

We have overlooked the improvement in gain that may be possible with directional antennas/adaptive beamforming and the effect of physical clutter. We will examine those effects as degradation or improvement factors in the signal processing. This means that problem that we must pursue is determining if it is possible to achieve through signal processing the detection of a target whose SDR is near -60 dB if we wish to pursue passive radar nets and even smaller if we wish for a passive radar to have the range of a short range surveillance radar. It is obvious that pursuit of passive radar nets will be easier to pursue. Thus, a SDR of about -60 dB is what we should be looking for in the analysis that follows.

CHAPTER 2: THE SCATTERING MODEL AND THE AMBIGUITY FUNCTION

This chapter discusses the scattering models that will be used in this thesis and their relation to the ambiguity function. The emphasis is on developing the correlation properties of the fields which are incident upon the receiver, and not upon detailed analysis of scattering cross sections. These properties will then be used to describe the output of the ambiguity function.

2.1 THE FM RADIO BROADCAST

The FM Radio broadcast uses voice and music signals to modulate the carrier signal. This is done through the use of instantaneous frequency. Suppose the voice and music signal is given by a(t) and that the carrier frequency is given by f_0. Then the modulation for a monophonic radio would be given by [6]:

$$v(t) = \cos(2\pi f_0 t + \kappa \int_{-\infty}^{t} a(t')dt' + \theta_0) \tag{2.1}$$

where κ is a constant called the frequency sensitivity which is used to spread the signal out over the given bandwidth. Now differentiating the argument of the cosine gives us the instantaneous frequency which yields:

$$\frac{1}{2\pi}\frac{d\theta}{dt} = f_0 + \kappa a(t) \tag{2.2}$$

Thus the instantaneous frequency is indeed modulated by the voice or music signal. Now real FM radio broadcasts are done in stereo so that a(t) is replaced by a multiplexed version of the sum and difference of the left and right speaker channels [6].

However, for the purposes of this thesis the importance of the FM radio modulation is that the transmitted signal can be expressed as a modulated time-harmonic wave as follows:

$$v(t) = \mathrm{Re}\{u(t)\exp(j2\pi f_0 t)\}$$
$$u(t) = \exp(j[\kappa \int_{-\infty}^{t} a(t')dt' + \theta_0]) \tag{2.3}$$

The modulation function, u(t), in the following analysis will be assumed to be a Gaussian random process with a Gaussian autocorrelation function. This assumption may not be valid in all cases, however, experimental evidence presented by Hall [4] suggests it can be made.

2.2 SCATTERING MODELS

We describe two scattering models. The first is the simple model which assumes one target. The second model will include multiple targets and can be extended to distributed targets.

First, we start by considering the single target model. We know the field at the transmitting antenna is given by equation 2.3 which means that we can solve for the harmonic amplitude terms at zero range:

$$E(\mathbf{0},t) = \frac{1}{2\pi}\int_{-\infty}^{\infty} E(\mathbf{0},\omega)\exp(j\omega t)d\omega = u(t)\exp(j\omega_0 t)$$
$$E(\mathbf{0},\omega) = U(\omega - \omega_0) \tag{2.4}$$

Next, since the radio antenna can be modeled as a collection of oscillating dipoles with field pattern $f_t(\hat{\mathbf{i}})$ the plane wave approximation can be used. This allows the time-harmonic wave to be written at the target a distance R_1 from the transmitter as indicated

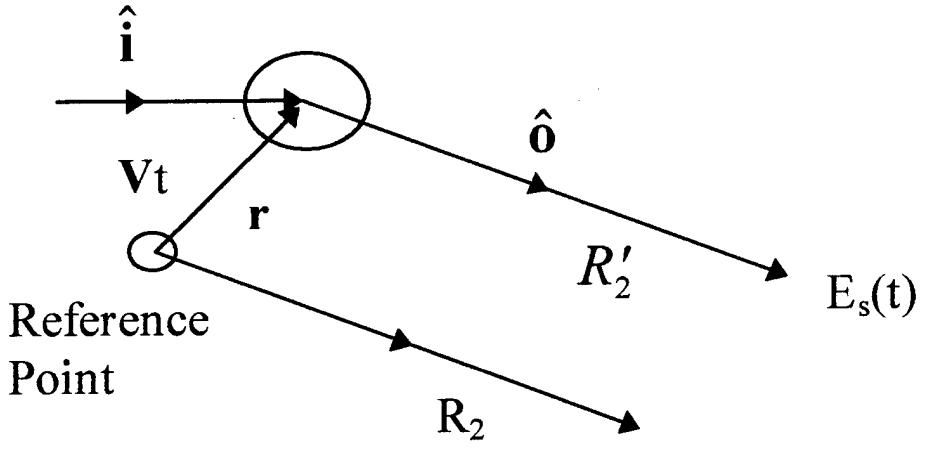

Figure 2.1: Geometry for a single moving target showing the directions of the incident wave $\hat{i}$, scattered wave $\hat{o}$, and the motion of the particle from a reference point with velocity **V** [7].

in figure 1.4 as:

$$E(R_1,\omega,\hat{\mathbf{i}}) = U(\omega-\omega_0)\frac{\exp(-jkR_1)}{R_1} f_t(\hat{\mathbf{i}}) \tag{2.5}$$

The wave is then scattered from the target as indicated in figure 2.1 with scattering amplitude $f_s(\hat{\mathbf{o}},\hat{\mathbf{i}})$. This allows the field at the receiver to be written as:

$$E(R_1,R_2,\omega,\hat{\mathbf{i}},\hat{\mathbf{o}}) = U(\omega-\omega_0)\frac{\exp(-jk(R_1+R_2))\exp(-j\mathbf{k}_s\cdot\mathbf{r})}{R_1R_2} f_t(\hat{\mathbf{i}})f_s(\hat{\mathbf{o}},\hat{\mathbf{i}})f_r(\hat{\mathbf{o}}) \tag{2.6}$$

where R_2 is the range from the target to the receiver, $\mathbf{k}_s = k(\hat{\mathbf{i}}-\hat{\mathbf{o}})$, **r** is the displacement vector from the reference point as in figure 2.1, and $f_r(\hat{\mathbf{o}})$ is the receiving pattern [7]. Now since $U(\omega-\omega_0)$, the baseband modulation, is approximately gaussian with a width of 30 kHz for FM broadcasts, the narrowband approximation that the scattering amplitudes and antenna patterns are the constant can be made [7]. Next, since $k= \omega/c$, we separate

2.6 into three parts:

$$E(R_1, R_2, \omega, \hat{\mathbf{i}}, \hat{\mathbf{o}}) = U(\omega - \omega_0)\exp\left[-j\omega\left(\frac{R_1 + R_2 + \hat{\mathbf{r}}_s \cdot \mathbf{r}}{c}\right)\right]\alpha \qquad (2.7)$$

Where α is the scattering amplitude divided by the range and $\hat{\mathbf{r}}_s = \hat{\mathbf{i}} - \hat{\mathbf{o}}$. Now we take the inverse fourier transform to get the field as a function of time at the receiver:

$$E(R_1, R_2, \hat{\mathbf{i}}, \hat{\mathbf{o}}, t) = \alpha u\left(t - \frac{R_1 + R_2 + \hat{\mathbf{r}}_s \cdot \mathbf{r}}{c}\right)\exp(j\omega_0 t)\exp(-jk_0(R_1 + R_2))\exp(-jk_0\hat{\mathbf{r}}_s \cdot \mathbf{r}) \qquad (2.8)$$

Now mixing this signal and making the approximation that $\hat{\mathbf{r}}_s \cdot \mathbf{r} << R_1, R_2$ allows it to be written as:

$$\alpha u\left(t - \frac{R_1 + R_2}{c}\right)\exp(-jk_0(R_1 + R_2))\exp(-jk_0\hat{\mathbf{r}}_s \cdot \mathbf{r}) \qquad (2.9)$$

Since **r** is the time-varying displacement vector from the reference point in figure 2.1, it follows that if we let t= 0 be the time when **r** = 0 then if the objects velocity is **V** it is possible to write the third term as $\exp(-jk_0\hat{\mathbf{r}}_s \cdot \mathbf{V}t)$ which is the bistatic doppler shift. With this change and the addition of the direct signal and the receiver noise the single scatter model is given by:

$$x(t) = \beta u(t - \frac{L}{c})\exp(-jk_0R_d) + \alpha u(t - \frac{R_s}{c})\exp(-jk_0R_s)\exp(-jk_0\hat{\mathbf{r}}_s \cdot \mathbf{V}t) + n(t) \qquad (2.10)$$

where $\beta = \frac{f_t(\hat{\mathbf{i}}')f_r(-\hat{\mathbf{i}}')}{L}$ with $\hat{\mathbf{i}}'$ being the unit vector of the direct line of site between transmitter and receiver, L being the baseline, $R_s = R_1 + R_2$ called the range sum, and n(t) being the receiver noise.

The scattering by multiple targets is simply the sum of the scatter by the targets given by equation 2.9, the direct signal, and the receiver noise since the scattered fields are added as vectors. This means that the measured field can be written as:

$$x(t) = \beta u(t - \frac{L}{c}) \exp(-jk_0 L) + \sum_i \alpha_i u(t - \frac{R_{si}}{c}) \exp(-jk_0 R_{si}) \exp(-jk_0 \hat{\mathbf{r}}_{si} \cdot \mathbf{V}t) + n(t) \qquad (2.11)$$

An important assumption that will be made in this thesis that has been shown experimentally to be true is that the correlation between scattered fields at different ranges is zero.

The previous model does not account for targets which are distributed in range and it does not account for the changing environment. The first of these problems can be handled by changing the summation to an integration. The second requires that the coefficient of the modulation signal, $u(t-R_s/c)$, in equation 2.11 be replaced by a quantity called the scattering amplitude, $\Phi(R_s,t)$, which is a random variable. Its value at any given time at particular range is given by the targets that are there. Now this means it is possible to write the measured field as:

$$x(t) = \beta u(t - \frac{L}{c}) \exp(-jk_0 L) + \int_{R_d}^{\infty} \Phi(R_s, t) u(t - \frac{R_s}{c}) dR_s + n(t) \qquad (2.12)$$

The variation in phase due to doppler shift means that over long time periods the scattering amplitude goes to zero. Also, it will go to zero because of range migration. These properties along with those given above can be summarized as follows:

$$\begin{aligned} &\langle \Phi(R_s, t) \rangle \approx 0 \\ &\langle \Phi(R_{s1}, t) \Phi^*(R_{s2}, t - \tau) \rangle \approx 0 \\ &\langle \Phi(R_{s1}, t) \Phi^*(R_{s1}, t - \tau) \rangle \approx \frac{\lambda^2 G_t(\hat{\mathbf{i}}) G_r(\hat{\mathbf{o}}) \sigma_{bi}(\hat{\mathbf{i}}, \hat{\mathbf{o}})}{(4\pi)^3 R_1^2 R_2^2} \exp(-jk_0 \hat{\mathbf{r}}_s \cdot \mathbf{V}\tau) \end{aligned} \qquad (2.13)$$

Notice that the time-correlated scattering amplitude is the radar equation 1.1 normalized by the transmitter power times the bistatic phase shift due to the target's motion. The bistatic phase shift is the result of the bistatic doppler shift of the target.

2.3 THE AMBIGUITY FUNCTION

The ambiguity function is the output of a filter matched to a delayed, doppler shifted version of the transmitter wave. It is a function of range, r, and doppler frequency, ν, with the ideal shape of the self-ambiguity function being a delta function at the origin. The following is a slightly modified version taken from Levanon [8]:

$$\left|\chi(r,\nu)\right| = \left|\int_{-\infty}^{\infty} y(t)x^*(t-r)\exp(-j2\pi\nu t)dt\right| \tag{2.14}$$

Notice that it looks nearly like the fourier transform in doppler, except it is a function of range. Indeed if we define the yx sequence as being:

$$yx_r(t) = y(t)x^*(t-r) \tag{2.15}$$

then for a constant range the ambiguity function is the fourier transform of the yx sequence. Now if we square the ambiguity function then at a constant range we obtain the power spectrum of the yx sequence. Then it can be shown that the inverse fourier transform of the ambiguity function at a constant range results in the autocorrelation sequence of the yx - sequence [4]. This can also be shown through the Wiener-Khintchine theorem in the case of stochastic transmitter waveforms. The result is that the ambiguity function in the correlation domain is given by:

$$Q(r,\tau) = E\left\{yx_r(t)yx_r^*(t-\tau)\right\} = E\left\{y(t)y^*(t-\tau)x(t-\tau-r)x^*(t-r)\right\} \tag{2.16}$$

The yx sequence provides a natural way of interpreting the ambiguity function. The question then is what is the physical meaning of the yx sequence. The following will provide the answer in the case of a traditional pulse radar. Consider the scattered wave,

$$y(t) = \int_0^\infty \Phi(R,t)u(t-\frac{R}{c})dR + n(t) \tag{2.17}$$

and the transmitter waveform x(t) = u(t). Take the time average of the yx sequence:

$$\begin{aligned} R_{yx}(r) &= \langle y(t)x^*(t-r)\rangle = \left\langle \left(\int_0^\infty \Phi(R,t)u(t-\frac{R}{c})dR + n(t) \right) u^*(t-r) \right\rangle \\ &= \left\langle \int_0^\infty \Phi(R,t)u(t-\frac{R}{c})u^*(t-r)dR \right\rangle + \langle n(t)u^*(t-r)\rangle \\ &\approx \int_0^\infty \langle \Phi(R,t)\rangle \left\langle u(t-\frac{R}{c})u^*(t-r) \right\rangle dR = \int_0^\infty \langle \Phi(R,t)\rangle \hat{R}_{uu}(r-\frac{R}{c})dR \end{aligned} \tag{2.18}$$

where we have used the independence of the noise and transmitter waveform along with their zero mean value. Also, the independence of the transmitter waveform and the scattering amplitude was used. The average of the scattering amplitude is zero mean over long time intervals for moving targets because of the bistatic doppler shift. However, if the averaging is done only for relatively short intervals it is constant. The averaging over short intervals is coherent averaging. Since the noise and transmitter waveforms average to zero much quicker than the scattering amplitude, coherent averaging is useful. The sequence that results from coherent averaging at a particular range is samples of the convolution of the autocorrelation of the transmitter waveform with the scattering amplitude(s) of the target(s) at that range. Ideally, it is desired that this autocorrelation would be a delta function centered at the origin. This would mean the resulting sequence consists of samples of the scattering amplitude at the desired range. The power spectrum of these samples could then be computed to find the spectrum of the scattering amplitudes

of the target(s) at that range. This is what the ambiguity function does. In an ideal sense, the ambiguity function at a given range should give us estimates of the power spectrum of the target(s) at that range.

2.4 DISCRETE COMPUTATION OF THE AMBIGUITY FUNCTION

The computation of the square of the ambiguity function is easy to infer from the discussion above. First, we form the yx sequences from the data at the ranges of interest. Next, we perform coherent averaging which can also be thought of as low pass filtering of the yx sequences. This is then followed by computing the periodogram using block averaging. The block averaging step is called incoherent averaging in the radar community because it involves averaging power quantities which are phase independent. Figure 2.2 illustrates the discrete computation.

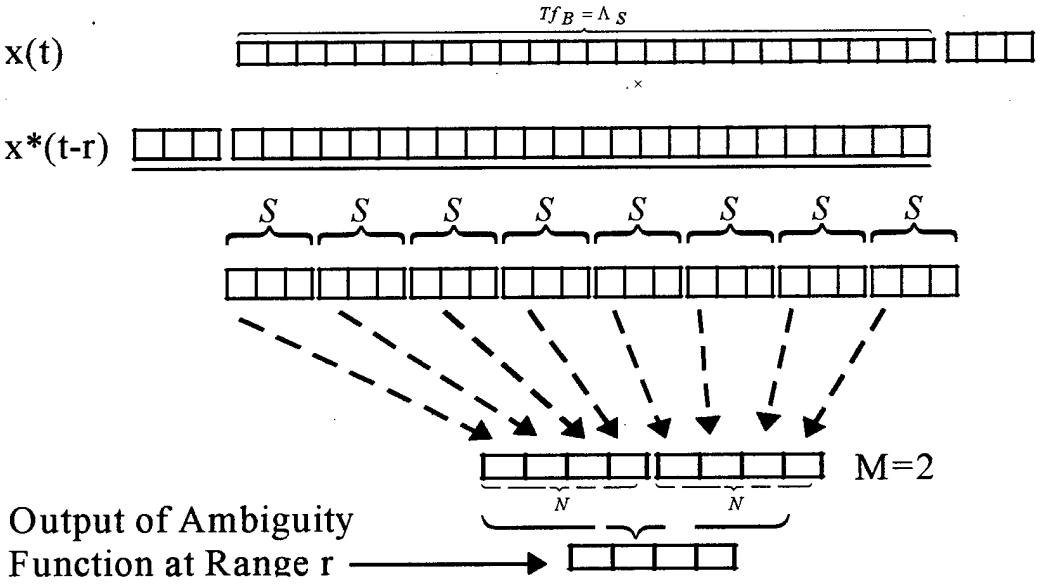

Figure 2.2: An illustration of the discrete computation of the ambiguity function at range r. Λ_S, is the length of the sequence (also will be defined as time-bandwidth product later), S is the number of coherent averages, M is the number of incoherent averages, and N is the number of Fourier frequencies.

CHAPTER 3: THE BIAS OF THE SELF AMBIGUITY FUNCTION

In this chapter we evaluate the bias of the self ambiguity function of the FM radio broadcast in the correlation domain. This can then be Fourier transformed to the frequency domain to give the bias of the self ambiguity function. By doing this, we learn about the general shape of the self ambiguity function of signal composed of a direct plus scattered signal. It is found that because the bias is concentrated origin of the self ambiguity function that it does not limit the sensitivity of the radar.

3.1 NOTATION

It is quite inconvenient to write out all the terms in equation 2.16 since 81 terms result when the received signal is described by equation 2.12. Instead, the following convention from section 2.3 will be adapted:

$$\begin{aligned} x(t) &= \beta u(t-\frac{L}{c})\exp(-jk_0 L) = \textit{direct signal} \\ y(t) &= \int_{R_d}^{\infty} \Phi(R_s,t)u(t-\frac{R_s}{c})dR_s = \textit{scattered signal} \\ n(t) &= \textit{noise} \end{aligned} \tag{3.1}$$

In the analysis of multiple receivers a subscript (1,2,..n) will denote the receiver. A capital X(t) means the sum of all three signals: X(t) = x(t) + y(t) + n(t). It too will have a numbered subscript in the case of multiple receivers.

For four-product correlations, it will be necessary to expand them out and use a simple convention for the four products which result. Consider the fourth-order

moment:

$$< \overbrace{(x(t)+y(t)+n(t))}^{X(t)} \overbrace{(x(t-r)+y(t-r)+n(t-r))^*}^{X^*(t-r)} \overbrace{(x(t-\tau)+y(t-\tau)+n(t-\tau))^*}^{X^*(t-\tau)}$$
$$\overbrace{(x(t-r-\tau)+y(t-r-\tau)+n(t-r-\tau))}^{X(t-r-\tau)} > \tag{3.2}$$
$$m_{1111} = \langle x(t)x^*(t-r)x^*(t-\tau)x(t-r-\tau)\rangle$$
$$m_{1213} = \langle x(t)y^*(t-r)x^*(t-\tau)n(t-r-\tau)\rangle$$

The two terms m_{1111} and m_{1213} are the examples of the notation used for the four product terms. Notice that an index being one indicates it is the direct signal, two indicates the scattered signal, and three means the noise term. The position of the index indicates the time shift of the term with the first index having no shift, the second being shifted by the range r, the third by autocorrelation lag τ, and the fourth by both range and autocorrelation lag.

The final simplification is to represent an autocorrelation as $R_{uu}(\tau)$ where the subscript is the random variable which is being correlated.

3.2 THE BIAS OF THE SELF-AMBIGUITY FUNCTION

To evaluate the bias of the self-ambiguity function in the correlation domain we must evaluate:

$$\hat{Q}(r,\tau) = < (x(t)+y(t)+n(t))(x(t-r)+y(t-r)+n(t-r))^*(x(t-\tau)+y(t-\tau)+n(t-\tau))^* \tag{3.3}$$
$$(x(t-\tau-r)+y(t-\tau-r)+n(t-\tau-r)) >$$

Instead of writing down all 81 four products it is easier to first identify terms which go to zero. To do this let us review the assumptions being made:

1) The noise and the transmitter waveform are zero mean random variables. This means the gaussian moment theorem may be applied

[4], namely the second moment of the same variable without conjugation on one goes to zero, third moments are zero, and the fourth moment with two conjugated variables may be expanded using equation 2.29, otherwise they are zero as well.

2) All three random variables: the noise, the transmitter waveform, and the scattering amplitude are independent of each other.

3) The averaging time is long enough so that any product of the scattering amplitude involving an odd number of terms or an odd number of conjugations will go to zero. This is a result of the doppler shift of the moving target. This *does not* apply to stationary targets. However, we ignore these since the power spectrum should allow us to distinguish moving targets from them.

We use these assumptions to eliminate terms in equation 3.3. Notice the third term of the received signal is noise. Using this combined with the assumptions above means the following 48 terms average to zero:

m_{1113}, m_{1123}, m_{1131}, m_{1132}, m_{1213}, m_{1223}, m_{1231}, m_{1232}, m_{1311}, m_{1312}, m_{1321}, m_{1322}, m_{1331}, m_{1332}, m_{1333}, m_{2113}, m_{2123}, m_{2131}, m_{2132}, m_{2213}, m_{2223}, m_{2231}, m_{2232}, m_{2311}, m_{2312}, m_{2321}, m_{2322}, m_{2331}, m_{2332}, m_{2333}, m_{3111}, m_{3112}, m_{3113}, m_{3121}, m_{3122}, m_{3123}, m_{3133}, m_{3211}, m_{3212}, m_{3213}, m_{3221}, m_{3222}, m_{3223}, m_{3233}, m_{3313}, m_{3323}, m_{3331}, m_{3332}

The scattering amplitude appears only in the scattered signal so we can eliminate 18 more:

m_{1112}, m_{1121}, m_{1211},m_{1221}, m_{1222}, m_{1233}, m_{1323}, m_{2111}, m_{2112}, m_{2122}, m_{2133}, m_{2212} m_{2221}, m_{2313}, m_{3132}, m_{3231}, m_{3312}, m_{3321}

This reduces the problem to the following 15 four products; notice that every subscript appears two or four times:

m_{1111}, m_{1122}, m_{1133}, m_{1212}, m_{1313}, m_{2121}, m_{2211}, m_{2222}, m_{2233}, m_{2323}, m_{3131}, m_{3232}, m_{3311}, m_{3322}, m_{3333}

Unfortunately, all these terms must be evaluated. First, let's look at the terms not requiring the use of the gaussian moment theorem. These all involve the autocorrelation of the noise times either a correlation of the scattered or direct signal. The terms are:

$$
\begin{aligned}
m_{1133} &= m_{3311}^{*} = \langle x(t)x^{*}(t-r)\rangle\langle n^{*}(t-\tau)n(t-\tau-r)\rangle = |\alpha|^{2} R_{uu}(r)R_{nn}(-r) \\
m_{1313} &= m_{3131}^{*} = \langle x(t)x^{*}(t-\tau)\rangle\langle n^{*}(t-r)n(t-r-\tau)\rangle = |\alpha|^{2} R_{uu}(\tau)R_{nn}(-\tau) \\
m_{2233} &= m_{3322}^{*} = \langle y(t)y^{*}(t-r)\rangle\langle n^{*}(t-\tau)n(t-\tau-r)\rangle = \left(\int_{R_d}^{\infty} R_{\Phi\Phi}(R_s,r)R_{uu}(r)dR_s\right)R_{nn}(-r) \qquad (3.4) \\
m_{2323} &= m_{3232}^{*} = \langle y(t)y^{*}(t-\tau)\rangle\langle n^{*}(t-r)n(t-r-\tau)\rangle = \left(\int_{R_d}^{\infty} R_{\Phi\Phi}(R_s,\tau)R_{uu}(\tau)dR_s\right)R_{nn}(-\tau)
\end{aligned}
$$

Since the autocorrelation at a positive lag is equivalent to the complex conjugate of the autocorrelation at the negative lag we see that the terms above appear in conjugate pairs. This means that when summed the bias due to these terms only occurs in the real part of the estimate of the autocorrelation function of the scattering amplitude. When the autocorrelation lags are Fourier transformed to the frequency domain this clutter should be symmetric about the range axis.

The last seven terms: m_{1111}, m_{1122}, m_{1212}, m_{2121}, m_{2211}, m_{2222}, m_{3333} all require the use of the gaussian moment theorem. The first six terms require that it be used on the four product of the transmitter waveform and the last term requires its use on the noise. The use of the scattering amplitude being uncorrelated at different ranges will also be used. Finally, there is no need to calculate m_{2222} since it is the four product of the scattered wave so the small value of the scattering amplitude to the fourth power eliminates it. We are left with:

$$
\begin{aligned}
m_{1111} &= |\alpha|^4 |R_{uu}(r)|^2 + |\alpha|^4 |R_{uu}(\tau)|^2 \\
m_{1122} &= |\alpha|^2 \int_{R_d}^{\infty} R_{\Phi\Phi}(R_s,-r)\left[|R_{uu}(r)|^2 + \left|R_{uu}(\tau - \frac{L-R_s}{c})\right|^2 \right] dR_s \\
m_{1212} &= |\alpha|^2 \int_{R_d}^{\infty} R_{\Phi\Phi}(R_s,-\tau)\left[\left|R_{uu}(r - \frac{L-R_s}{c})\right|^2 + |R_{uu}(\tau)|^2 \right] dR_s \\
m_{2121} &= |\alpha|^2 \int_{R_d}^{\infty} R_{\Phi\Phi}(R_s,\tau)\left[\left|R_{uu}(r - \frac{R_s-L}{c})\right|^2 + |R_{uu}(\tau)|^2 \right] dR_s \\
m_{2211} &= |\alpha|^2 \int_{R_d}^{\infty} R_{\Phi\Phi}(R_s,r)\left[|R_{uu}(r)|^2 + \left|R_{uu}(\tau - \frac{R_s-L}{c})\right|^2 \right] dR_s \\
m_{3333} &= |R_{nn}(r)|^2 + |R_{nn}(\tau)|^2
\end{aligned}
\tag{3.5}
$$

The terms which correspond to the target are m_{1212} & m_{2121}. If the transmitter waveform is nearly a delta function, then m_{2121} should yield an estimate of the autocorrelation lags of the range of interest and m_{1212} yields the complex conjugate of the autocorrelation lags at the negative range of the target. This is the hermite symmetry of the self ambiguity function [8]. The terms m_{2211} & m_{1122} result from the interchangability of the range and the lag terms. Notice there is a hermite symmetry present here as well. This will be easy to notice in the following plots of ambiguity functions. The final terms are the self-correlation of the direct signal and the noise.

We can now determine the bias of the self ambiguity function. Because of the bandwidth of the FM radio broadcast (~ 30 kHz), we know that the autocorrelation function of the baseband modulation is a sharp peak. This means that all terms whose arguments are either τ or r must be concentrated either on the lag or range axis respectively. From equations 3.4 and 3.5 it is apparent this is every term except those involving the target(s) or its hermite counterpart. When Fourier transformed, the bias due to the clutter on the lag axis results in a constant being added to the clutter floor, and the bias on the range axis results in the spike of the self-ambiguity function at zero range and Doppler. This means that the bias of the self-ambiguity function will not affect the

detection of a target which is not on the receiver transmitter baseline. We verified this result by carrying out simulations which injected a target into sampled FM broadcasts and trying techniques which can be derived from the analysis above to reduce the bias. In all cases, the results showed that there was no difference between biased self-ambiguity function estimate and the estimate whose bias we had reduced. This means that the sensitivity of the radar is determined not by the bias, but instead is determined by the variance of the self-ambiguity function. We discuss this problem in the next chapter.

CHAPTER 4

THE PROBABILITY DISTRIBUTION OF THE SELF AMBIGUITY FUNCTION

The last chapter indicated that the sensitivity of the bistatic FM radar is independent of the bias of the self ambiguity function. Instead, it depends upon the variance of the clutter floor of the self ambiguity function. If we were to pursue the variance through the technique of last chapter, the combinatoric blossoming of terms would quickly overwhelm us. However, if we make the additional assumption that the signal's spectrum is white it is possible to arrive at a useful description of the self ambiguity function's probability distribution. We can then make phenomenological adjustments for the case of the FM radio broadcast. In addition, knowing the self ambiguity function's probability distribution also allows a performance analysis of the radar to be made, and it provides a way to determine the threshold for automatic detection systems.

4.1 DERIVATION OF THE PROBABILITY DENSITY OF THE CLUTTER FLOOR

Calculating the probability density of the self ambiguity function seems a daunting task considering the steps needed to determine the bias of the ambiguity function for a gaussian signal. However, if we make the following two assumptions about the received signal then it will be possible arrive at a theoretical model that can be compared to experimental results.

1) The process is white which means $E\{x(t)x^*(t-r)\} = 0$ for $r \neq 0$.

2) The real and imaginary terms of x(t) are uncorrelated and Gaussian distributed with zero mean.

These two assumptions mean the in-phase (real) component $x_i(t)$ and the quadrature (imaginary) component $x_q(t)$ are independent of each other and are independent of themselves except for r=0.

To calculate the probability density of the clutter floor of the we first consider just the direct signal. Form the new sequence $a(t) = x(t)x^*(t-r)$, where r is the range variable which is greater than zero. Consider the mean of the new sequence:

$$E\{x_i(t)x_i(t-r) + x_q(t)x_q(t-r) + j\left[x_q(t)x_i(t-r) - x_i(t)x_q(t-r)\right]\} = 0 \qquad (4.1)$$

which follows from the independence of the zero mean gaussian random variables. Next consider the variance of the in-phase component of a(t):

$$\begin{aligned} &\text{var}\{a_i(t)\} = E\{(x_i(t)x_i(t-r)+x_q(t)x_q(t-r))^2\} = \\ &E\{x_i(t)^2x_i(t-r)^2+2x_i(t)x_i(t-r)x_q(t)x_q(t-r)+x_q(t)^2x_q(t-r)^2\} = \\ &E\{x_i(t)^2\}E\{x_i(t-r)^2\}+2E\{x_i(t)\}E\{x_i(t-r)\}E\{x_q(t)\}E\{x_q(t-r)\}+E\{x_q(t)^2\}E\{x_q(t-r)^2\} = 2\sigma^4 \end{aligned} \qquad (4.2)$$

Where the last two steps follow from independence and the assumption the random variables are $N(0,\sigma)$. It can be similarly shown that:

$$\text{var}\{a_q(t)\} = 2\sigma^4 \qquad (4.3)$$

Next, we show that the real and imaginary components of a(t) are uncorrelated:

$$\begin{aligned} &corr\{a_i(t),a_q(t')\} = E\{a_i(t)a_q(t')\} = E\{x_i(t)x_i(t-r)x_q(t')x_i(t'-r) - \\ &x_i(t)x_i(t-r)x_i(t')x_q(t'-r) + x_q(t)x_q(t-r)x_q(t')x_i(t'-r) - \\ &x_q(t)x_q(t-r)x_i(t')x_i(t'-r)\} = 0 \end{aligned} \qquad (4.4)$$

Where the last step follows from the independence and zero mean of the random variables and holds for all sets of (t,t′) including t = t′. Finally, we show that real and

imaginary components are uncorrelated with respect to themselves except for t = t′. We show the proof for the real part only since its similar for the imaginary component.

$$\begin{aligned} &E\{(x_i(t)x_i(t-r)+x_q(t)x_q(t-r))(x_i(t')x_i(t'-r)+x_q(t')x_q(t'-r))\} = \\ &E\{x_i(t)x_i(t-r)x_i(t')x_i(t'-r)+x_i(t)x_i(t-r)x_q(t')x_q(t'-r)+ \qquad t\neq t' \\ &x_q(t)x_q(t-r)x_i(t')x_i(t'-r)+x_q(t)x_q(t-r)x_q(t')x_q(t'-r)\} = 0 \end{aligned} \tag{4.5}$$

The result follows from the requirement that r≠0. In this case the only way there could be a nonzero term is if the following two equations are satisfied:

$$\begin{aligned} t &= t'-r \\ \underline{-t' &= t-r} \\ t-t' &= t'-t \Rightarrow t = t' \end{aligned}$$

which is what we wanted to show.

With these properties of a(t) in mind we proceed in a manner quite similar to the computation of the probability density of the spectral density function given in Percival pages 220-223 [9]. First, we note from chapter 2 that the ambiguity function is the power spectrum of a(t). This is estimated through the periodogram which we define as [10]:

$$S(f) = \left| \sum_{n=0}^{N-1} a(t) \exp\left(\frac{-j2\pi ft}{N}\right) \right|^2 \tag{4.6}$$

We expand the inner summation into its real and imaginary components:

$$\begin{aligned} &\sum_{t=0}^{N-1} a(t)\exp\left(\frac{-j2\pi ft}{N}\right) = \sum_{t=0}^{N-1}\left[a_i(t)\cos\left(\frac{2\pi ft}{N}\right)+a_q(t)\sin\left(\frac{2\pi ft}{N}\right)\right]+ \\ &j\sum_{t=0}^{N-1}\left[a_q(t)\cos\left(\frac{2\pi ft}{N}\right)-a_i(t)\sin\left(\frac{2\pi ft}{N}\right)\right] = A(f)+jB(f) \end{aligned} \tag{4.7}$$

This means $S(f) = A(f)^2+B(f)^2$. Now we wish to show that A(f) and B(f) are independent Gaussian random variables over the set of fourier frequencies (f an integer between 0 and N-1). To do this we first show that A(f) and B(f) are uncorrelated over the Fourier frequencies.

$$corr\{A(f),B(f')\} = E\{A(f)B(f')\} = E\left\{\left(\sum_{t=0}^{N-1} a_i(t)\cos\left(\frac{2\pi ft}{N}\right)+a_q(t)\sin\left(\frac{2\pi ft}{N}\right)\right)\right.$$
$$\left.\left(\sum_{t'=0}^{N-1} a_q(t')\cos\left(\frac{2\pi f't'}{N}\right)-a_i(t')\sin\left(\frac{2\pi f't'}{N}\right)\right)\right\} = E\left\{\sum_{t'=0}^{N-1}\sum_{t=0}^{N-1}\left[a_i(t)a_q(t')\cos\left(\frac{2\pi ft}{N}\right)\cos\left(\frac{2\pi f't'}{N}\right)-\right.\right.$$
$$a_i(t)a_i(t')\cos\left(\frac{2\pi ft}{N}\right)\sin\left(\frac{2\pi f't'}{N}\right)+a_q(t)a_q(t')\sin\left(\frac{2\pi ft}{N}\right)\cos\left(\frac{2\pi f't'}{N}\right)- \qquad (4.8)$$
$$\left.\left.a_q(t)a_i(t')\sin\left(\frac{2\pi ft}{N}\right)\cos\left(\frac{2\pi f't'}{N}\right)\right]\right\} = \sum_{t=0}^{N-1}\left[2\sigma^4\cos\left(\frac{2\pi ft}{N}\right)\sin\left(\frac{2\pi f't}{N}\right)\right]+$$
$$\sum_{t=0}^{N-1}\left[2\sigma^4\sin\left(\frac{2\pi ft}{N}\right)\cos\left(\frac{2\pi f't}{N}\right)\right] = 0$$

The third step follows from 4.3, 4.4, 4.5, and the linearity of the expectation operator. The final step involves the use of the relation derived in exercise 1.4 of Percival [9]:

$$\sum_{t=0}^{N-1}\left[\cos(2\pi ft)\sin(2\pi f't)\right] = \frac{1}{4j}\sum_{t=0}^{N-1}\left[\exp(j2\pi t(f'+f))-\exp(-j2\pi t(f'+f))+\right.$$
$$\left.\exp(-j2\pi t(f-f'))-\exp(j2\pi t(f-f'))\right] = S_N(f-f')+S_N(f+f'). \qquad (4.9)$$
$$S_N(f) = \frac{N}{2}\frac{\sin(N\pi f)}{N\sin(\pi f)}\sin((N-1)\pi f) = \frac{N}{2}D_N(f)\sin((N-1)\pi f)$$

where $D_N(f)$ is one form of Dirichlet's kernel. Since we are interested in the frequencies between 0 and N-1 it follows from 4.9 that 4.8 is zero. This is for all except f = 0, but we are not interested in it since we expect our targets to have some motion. This shows that that A(f) and B(f) are uncorrelated for any combination of fourier frequencies except for f,f' = 0.

Next, we show that A(f) and B(f) are Gaussian distributed using the Central Limit Theorem. The Central Limit theorem states that the sum of n independent random variables tends towards a $N(\mu,\sigma)$ where $\mu=\mu_1+...+\mu_n$ and $\sigma^2=\sigma^2_1+...+\sigma^2_n$ as n approaches infinity [10]. This requires that we show the variables in the summation are independent. In the case of 4.7, this means it is necessary to justify that $a_i(t)$ is independent of $a_i(t')$ and similarly for $a_q(t)$. Consider $a_i(t)$:

$$\begin{aligned} a_i(t) &= x_i(t)x_i(t-r) + x_q(t)x_q(t-r) \\ a_i(t') &= x_i(t')x_i(t'-r) + x_q(t')x_q(t'-r) \end{aligned} \tag{4.10}$$

We offer the following heuristic justification based on conditional probability. It is necessary to show that knowledge of $a_i(t)$ does not increase our probability of guessing the value of $a_i(t')$. Since $t\neq t'$ it means $x_i(t')x_i(t'-r)$ is independent of $x_i(t)x_i(t-r)$ and $x_q(t)x_q(t-r)$ is independent of $x_q(t')x_q(t'-r)$. This follows from the fact that multiplying two independent random variables by a constant does not change their independence. Since this is true it quickly follows that $a_i(t)$ must be independent of $a_i(t')$. This reasoning can be extended to showing that all the random variables in the set $\{a_i(0)...a_i(N-1)\}$ are independent. We use the following Bayesian theorem of probability which states that [10]:

$$P(A_n \ldots A_1) = P(A_n \mid A_{n-1} \ldots A_1) \ldots P(A_2 \mid A_1) P(A_1) \tag{4.11}$$

where $A_n \ldots A_1$ are events which in the case of a random variable $A_i = \mathbf{x}_i \leq x_i$ which means $P\{A_i\}$ is simply the cumulative distribution of $\mathbf{x}_i$. Consider the case of N = 3. We have already shown that the random variables $a_i(0)$, $a_i(1)$, $a_i(2)$ are pairwise independent, but we must show:

$$P(\{a_i(0)\leq x_0\}\cap\{a_i(1)\leq x_1\}\cap\{a_i(2)\leq x_2\}) = P(\{a_i(0)\leq x_0\})P(\{a_i(1)\leq x_1\})P(\{a_i(2)\leq x_2\}) \tag{4.12}$$

This follows easily through adding an additional term $a_i(t'')$ to the two already present in 4.10. Notice that this third term contains a new random variable $a_i(t')$ which will be

independent of $a_i(t)$ and $a_i(t')$. Using equation 4.11 and this independence between terms it follows that 4.12 holds. This process can be continued inductively to show that the set $\{a_i(0)...a_i(N-1)\}$ is composed of independent random variables. Similarily, this can be shown to be true for $a_q(t)$.

Now we may apply the Central Limit Theorem to the four sums in 4.7. This means we have $A(f) \sim N\left(0,\sqrt{\sum_{t=0}^{N-1} 2\sigma^4 \cos^2\left(\frac{2\pi ft}{N}\right)}\right) + N\left(0,\sqrt{\sum_{t=0}^{N-1} 2\sigma^4 \sin^2\left(\frac{2\pi ft}{N}\right)}\right)$ and $B(f) \sim N\left(0,\sqrt{\sum_{t=0}^{N-1} 2\sigma^4 \cos^2\left(\frac{2\pi ft}{N}\right)}\right) + N\left(0,\sqrt{\sum_{t=0}^{N-1} 2\sigma^4 \sin^2\left(\frac{2\pi ft}{N}\right)}\right)$ where we have used the fact that the taking the negative of a zero mean gaussian random variable does not change its distribution. Combining the distributions of A(f) requires that the correlation between the two normal distributions be computed. However, this is easily seen to be zero since equation 4.4 shows that $a_i(t)$ and $a_q(t')$ are uncorrelated for any combination (t,t'). This obtains $A(f) \sim N(0,\sigma^2\sqrt{2N})$ and similarly it can be shown that $B(f) \sim N(0,\sigma^2\sqrt{2N})$.

Finally, we can determine the probability density of the self ambiguity function of a white Gaussian signal away from r = 0. First, we note that because A(f) and B(f) are uncorrelated and Gaussian they must be independent. Next, we scale A(f) and B(f) as $\frac{1}{\sigma^2\sqrt{2N}}A(f) \sim N(0,1)$ and $\frac{1}{\sigma^2\sqrt{2N}}B(f) \sim N(0,1)$. Now squaring the normalized variables results in two independent chi-square random variables with one degree of freedom [10]. Next, summing two independent chi-square random variables of one degree of freedom results in a chi-square random variable of two degrees of freedom. This gives:

$$\frac{1}{2N\sigma^4}\left|X(r,f)\right|^2 = \frac{1}{2N\sigma^4}S_r(f) = \frac{1}{2N\sigma^4}A(f)^2 + \frac{1}{2N\sigma^4}B(f)^2 \sim \chi_2^2 \qquad (4.13)$$

where we have used capital chi squared to represent the ambiguity function squared and the lowercase chi squared represents the chi-square distribution. Next, if incoherent averaging (block averaging with no overlap) is used it follows that the chi-square random variables from each block should be independent of each other, since the data from block to block is independent. This means the ambiguity function squared will have the following distribution:

$$\frac{M}{2N\sigma^4}\left|\mathrm{X}(r,f)\right|^2 = \frac{M}{2N\sigma^4}S_r(f) = \frac{M}{2N\sigma^4}[\frac{1}{M}\sum_{m=0}^{M-1}[A_m(f)^2 + B_m(f)^2] \sim \chi^2_{2M} \qquad (4.14)$$

Finally, we consider the effect of coherent averaging. In this case, $a_i(t)$ and $a_q(t)$ are being pre-averaged before being summed in 4.7. As long as the blocks of a(t) that are being pre-averaged do not overlap the independence relations hold, but the variance of $a_i(t)$ and $a_q(t)$ changes. The averaging is done as follows:

$$a_s(t) = \frac{1}{S}\sum_{s=0}^{S-1}a(tS+s) = \frac{1}{S}\sum_{s=0}^{S-1}a_i(tS+s) + ja_q(tS+s) \qquad (4.15)$$

where S is the length of the average. It follows that the semivariances of $a_s(t)$ are both equal to $2\sigma^4/S$. This means that to account for coherent integration 4.14 should be modified as follows:

$$\frac{MS}{2N\sigma^4}\mathrm{X}^2(r,f) = \frac{MS}{2N\sigma^4}S_r(f) = \frac{MS}{2N\sigma^4}[\frac{1}{M}\sum_{m=0}^{M-1}[A_m(f)^2 + B_m(f)^2] \sim \chi^2_{2M} \qquad (4.16)$$

4.1.2 COMPARISON TO SIMULATED DATA

Theory must agree with experimental evidence in order for a model to be useful. We start by examining whether 4.16 actually predicts the true behavior of the square of the ambiguity function. To begin, a complex sequence whose real and imaginary components are uncorrelated and gaussian distributed with zero mean and unit variance is generated in Matlab. Although it is not necessary to attach a sampling frequency, we use a frequency of 250 kHz since this is the sampling frequency of the experimental data that is presented later. The length, L, of the sequence that is analyzed is 131,072 points which means it is approximately a half second of data. The following is the plot of $|X(r,f)|^2$ using a coherent averaging factor S = 250, block size N=64, and the incoherent averaging factor M = 8. The incoherent averaging factor can be determined as $M = \lfloor L/(SN) \rfloor$ ($\lfloor \rfloor$ is the greatest integer less than or equal to the quantity in the brackets).

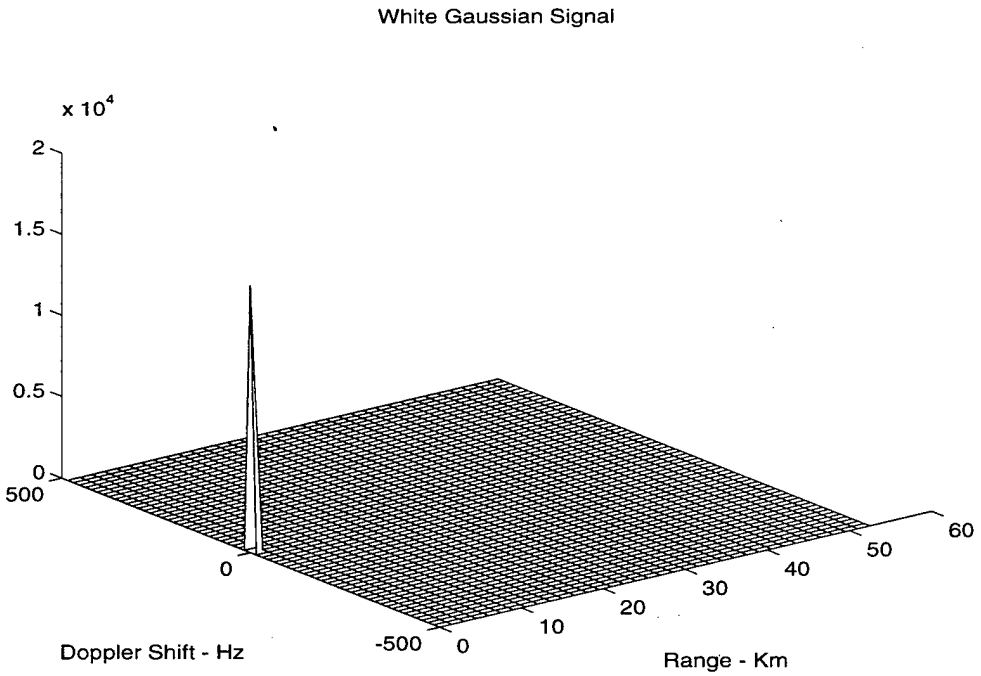

Figure 4.1: Plot of $|X(r,f)|^2$ of a White Gaussian Signal. Created from 0.52 seconds of data sampled at 250 kHz. Block size (N=64) and coherent integration factor (S=250).

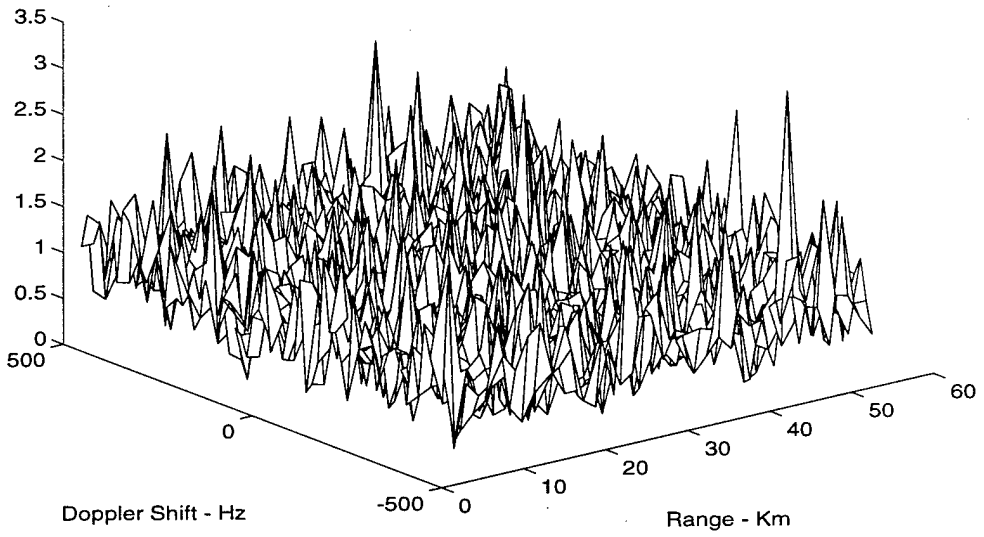

Figure 4.2: Same as Figure 4.1 except range 0 is not displayed. Shows clutter floor.

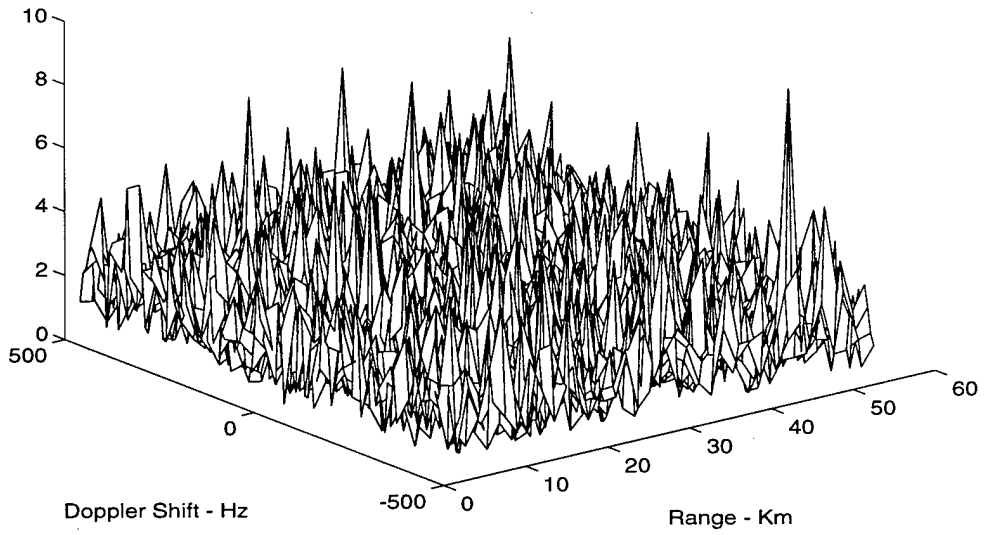

Figure 4.3: Plot of the clutter floor for same white gaussian signal except this time $|X(r,f)|^2$ was computed with N=128 and S= 250.

Figure 4.1 is the desired thumbtack appearance of the white gaussian signal. The next figure on the following page, figure 4.2, is the same plot except for all ranges greater than zero. This is the clutter floor that equation 4.16 should describe. Figure 4.3 is the plot of the clutter floor except this time the ambiguity function was computed with a different block size N=128. The next step is to compute the normalization factor and multiply it times the square of the ambiguity function. Then the histogram of the clutter of figure 4.2 is plotted versus the predicted chi-square random variable of 16 degrees of freedom in figure 4.4. Similarly, the clutter floor of figure 4.3 is plotted against a chi-square of 8 degrees of freedom in figure 4.5. The results appear to fit the distributions very closely which gives us confidence in equation 4.16.

However, an even better test for determining the closeness of a probability distribution to a theoretical model is to use the Kolmogroff-Smirnov (K-S) test [10]. The K-S test is a hypothesis test with null hypothesis that the distributions are equal and the alternative hypothesis is that they are different. The test statistic is:

$$\mathbf{q} = \max_{x} \left| \hat{\mathbf{F}}(x) - F_0(x) \right| \tag{4.17}$$

where $F_0(x)$ is the hypothesized cumulative distribution and $\hat{\mathbf{F}}(x)$ is the empirical estimate of the cumulative distribution. Estimating the cumulative distribution is done by first sorting the data into ascending order and then assigning the value of i/N to $\hat{\mathbf{F}}(x_i)$ where i is the position of the data point in the sorted sequence. N is the length of the sequence. Obviously, it follows from equation 4.17 that if the two distributions are equal then **q** should be near zero if a sufficient number of points, N, are used. This is expressed as [10]:

$$\text{Accept } H_0 \text{ iff } \mathbf{q} < \sqrt{\frac{-1}{2N} \ln \frac{\alpha}{2}} \tag{4.18}$$

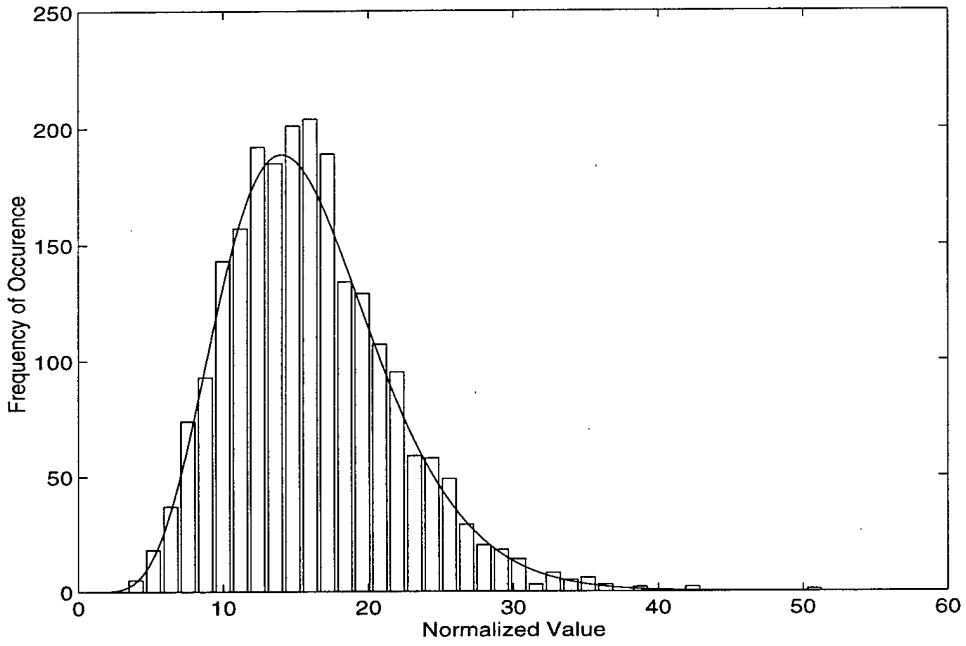

Figure 4.4: The histogram vs. the theoretical prediction, χ^2_{16}, for the data of figure 4.2.

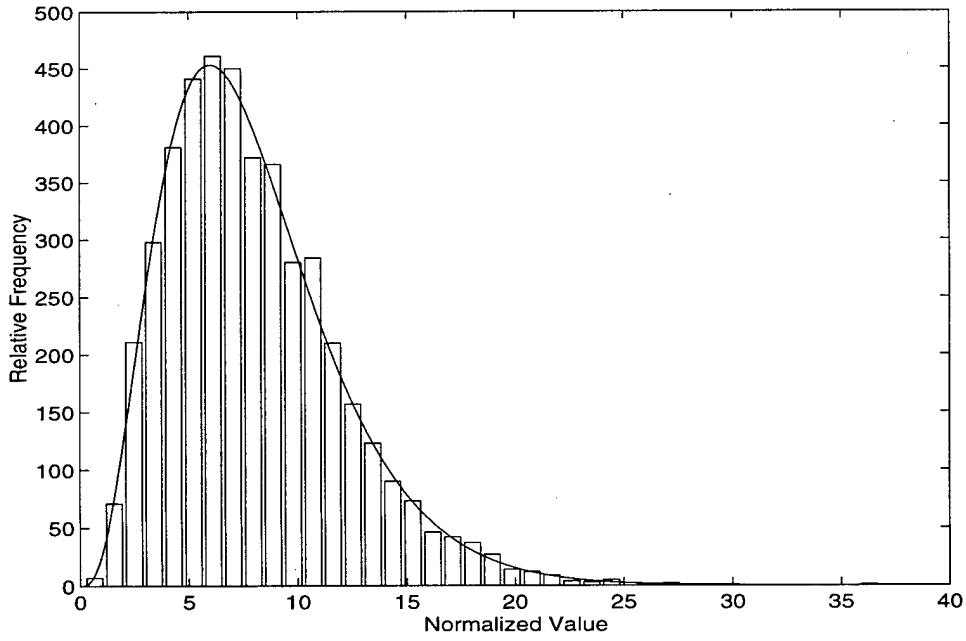

Figure 4.5: The histogram vs. the theoretical prediction, χ^2_8, for the data of figure 4.3.

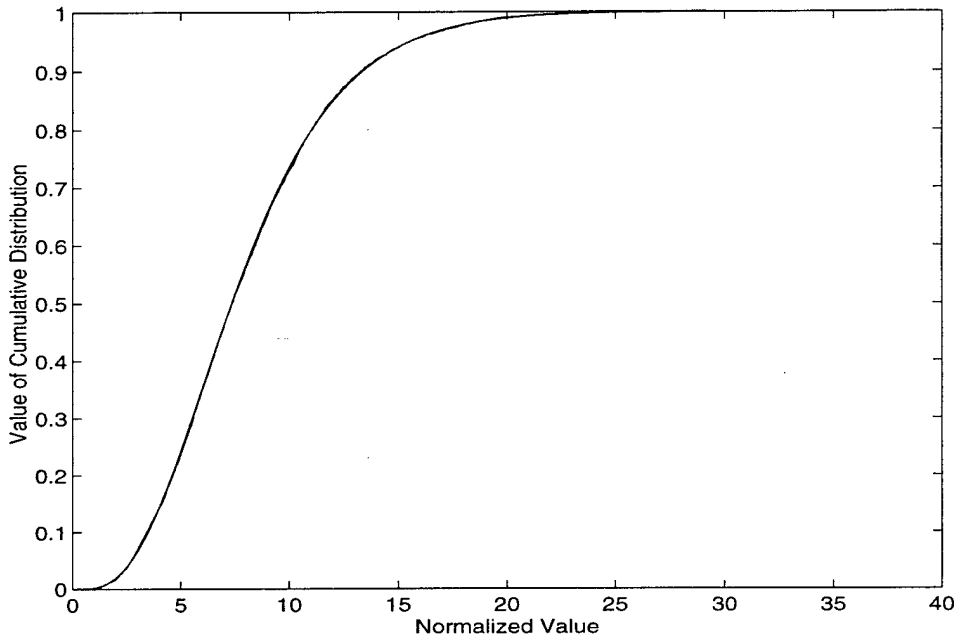

Figure 4.6: Plot of theoretical vs. empirical cumulative distribution function for data of figure 4.5, N=2,240. The two curves are essentially indistinguishable.

where $\alpha=P\{\mathbf{q}>c|H_0\} \approx 2e^{-2nc^2}$ is the significance level. A value of α near one indicates that we have correctly identified the distribution. Figure 4.6 shows that the empirical cumulative distribution of the data in figure 4.5 is essentially indistinguishable from the theoretical cumulative distribution of a χ_8^2. In this case, $\mathbf{q} = 0.00825$. A value so small that for all values of $\alpha<1$ it easily passes 4.18. This means we should accept the null hypothesis, and it gives strong justification that equation 4.16 correctly models the simulated data.

4.1.2 MODEL COMPARISON TO EXPERIMENTAL DATA

The data that will be used is six different samples each of length 0.5 seconds of FM radio broadcasts taken at a sampling frequency of 250 kHz. The broadcast stations that were sampled were A1=106.9, A2=93.3, A3=94.9, A4=94.9, A5=97.3, and

A6 = 97.3. A3 and A4 were sampled on different days as well as A5 and A6. The three sequences A1, A4, and A5 were sampled at approximately the same time on the same receiver, and the sequences A3 and A6 were also taken at nearly the same time on the same receiver. The purpose of choosing these samples was to ensure that any characteristics that could be due to receiver error could be identified by showing up in sequences taken at nearly the same time.

Before we begin the comparison to empirical data, we give a brief justification why we should expect similar behavior. The assumptions that the radio broadcast is white Gaussian noise is obviously incorrect. However, it is well known that the autocorrelation time of the broadcast is less than 10 μs [4]. Also, since the spectrum of the FM broadcasts are known to be approximately gaussian which implies symmetry about the carrier frequency, it can be shown that the in-phase and quadrature components are uncorrelated [2]. Thus, we appeal to the same argument that Percival uses to justify the density of the periodogram for non-white/non-gaussian processes which requires certain higher-order moments to be finite [9]. It applies because that analysis is being used here to determine the probability distribution of the ambiguity function, and because the FM waveform has finite moments of all positive orders [11].

First, we look at the ambiguity plots of the six sequences. The plots are all of $|X(r,f)|$ not its square since this makes the clutter problems more apparent. By range we mean the difference between the direct and scattered path. Also, the Doppler shift is given in Hz instead of velocity since the carrier frequencies change from station to station.

Out to about the range of 10 km there appears to be quite a bit of unexpected clutter in all the signals. Signals A1, A4, and A5 all have a strip of apparent clutter out to 50 km at zero doppler. Since the data was taken at different frequencies, it is probable that this is due to a constant DC offset in the receiver. However, if we look on either side of zero doppler the plot appears relatively flat. The flatness of the clutter plane also appears in A2 and A6. However, signal A3 appears to have considerable

clutter. A possible explanation for this is that it is known that the station at 94.9 MHz has its transmitter located on Capitol Hill which is only 1-2 km from the University where the data was collected. In contrast, the rest of the stations are known to have transmitters located further than 20 km away. However, we also know A4 is a sample of the station at 94.9 MHz, but does not appear to have the clutter at ranges greater than 10 km. One important difference is that A3 was generated at approximately 4 pm opposed to A4 which was sampled at 1 am. It is possible that the change in daily activity along with a possible change in the transmitting mode at night could make the difference.

With the clutter problems of the signal, we would not expect our model to hold for ranges less than 10 km. Additional inspection showed that there was still some clutter in the ranges out to 16.5 km. That the waveforms of the $|X(r,f)|^2$ resembled the clutter floor of the white Gaussian signal for this set of ranges can be seen in figures 4.10 - 4.12. Notice that there is still a bit of clutter in A1, A2, A4, A5, and A6 with a considerable amount present in A3. However, we continue by plotting the histograms of the data versus χ^2_{16}. One problem is proper normalization of the data. In the simulation, we controlled the variance of real and imaginary components of the signal, but here there is no control. This means it is quite likely that the real and imaginary components will have a different variance. Also, we know it is not a white noise process. This means the normalization constant calculated in 4.16 is incorrect because when summing the variances the cross correlation between terms must be included. Instead, we compute the normalization constant by forcing the mean of the data to take the same value as the mean of a χ^2_{16}. Since, the mean of a chi-square is equal to its degrees of freedom this is a simple procedure. The histograms can be seen in figure 4.13 on the following page. The number of data points used in each histogram is 806. Notice that there is definite mismatch for signal A3. However, A1, A4, and A5 also appear to have a problem with their means being located in the wrong place. The general shape of the histograms though appear close to the chi-square density. We gain confidence by looking at A2 and A6. Notice that

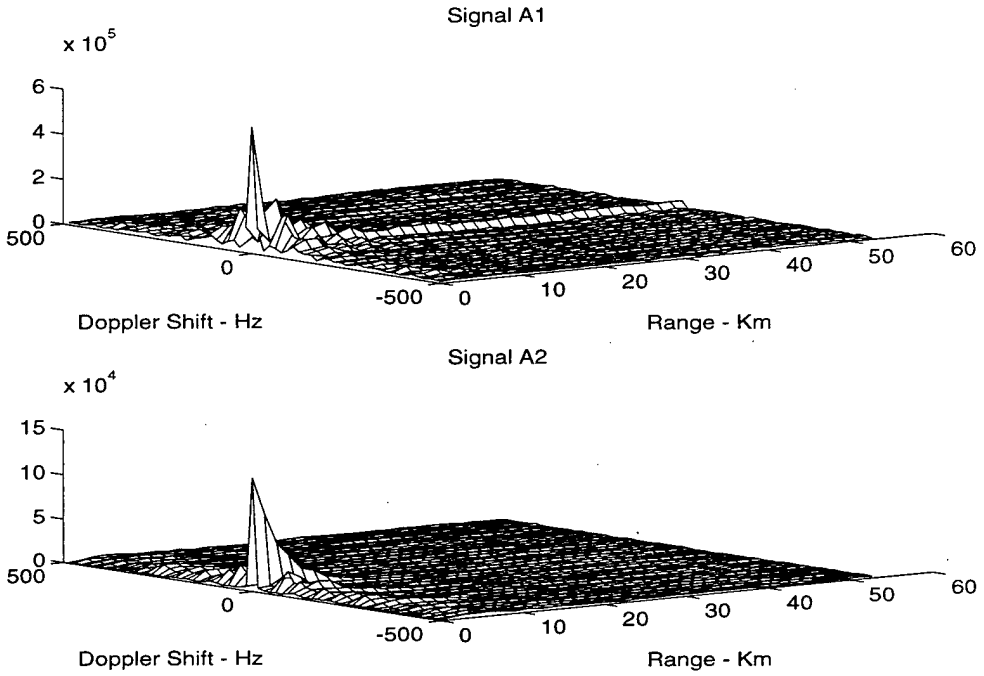

Figure 4.7: Mesh plots of |X(r,f)| of signals A1 = 106.9 Mhz & A2 = 93.3 Mhz sampled at different times.

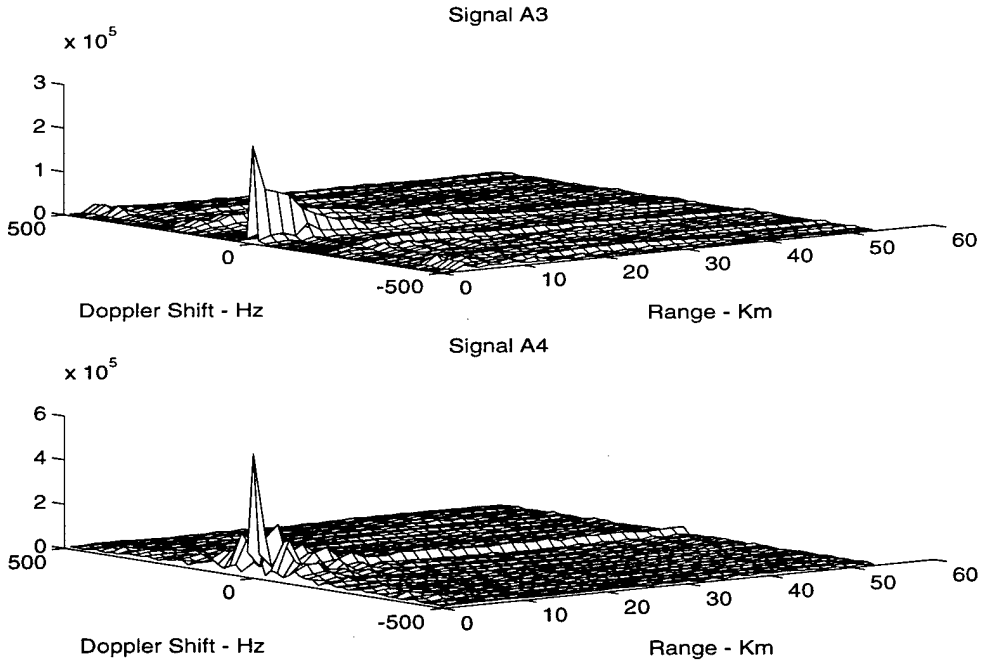

Figure 4.8: Mesh plots of |X(r,f)| of signals A3 = 94.9 Mhz & A4 = 94.9 Mhz sampled at different times.

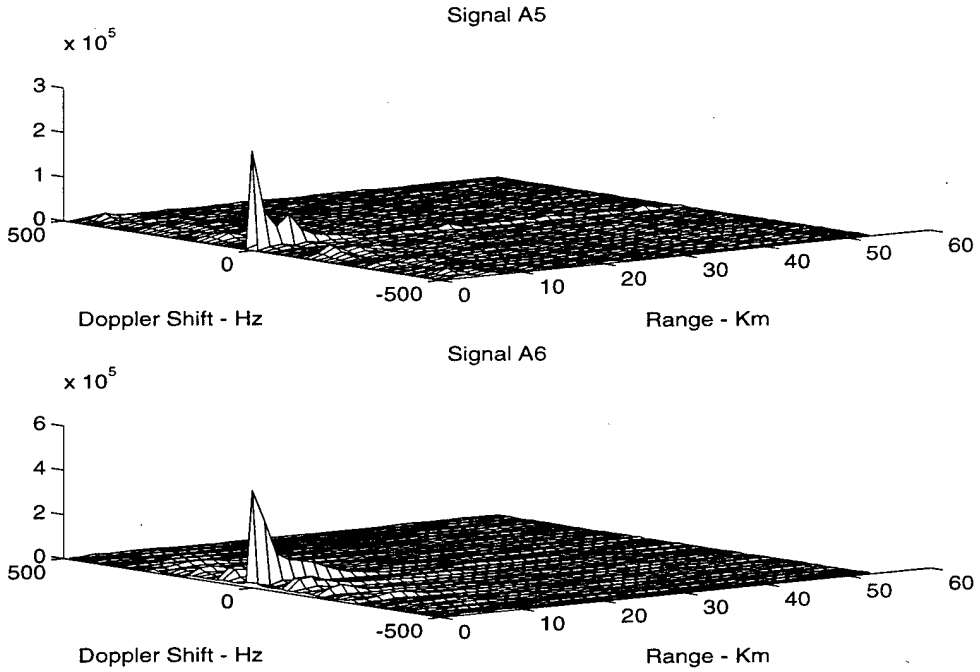

Figure 4.9: Mesh plots of |X(r,f)| of signals A5 = 97.3 Mhz & A6 = 97.3 Mhz sampled at different times.

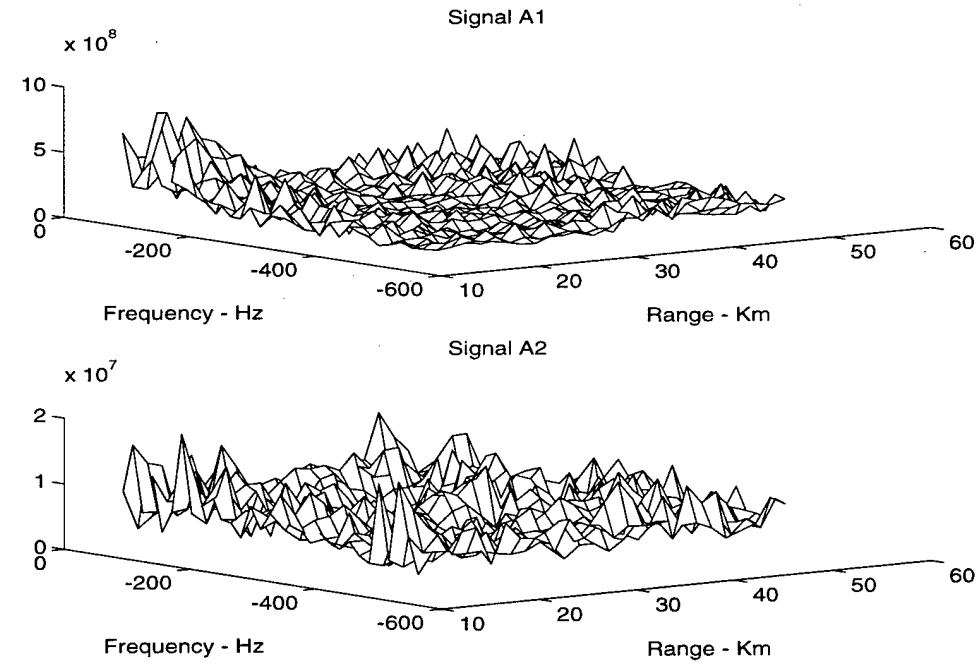

Figure 4.10: $|X(r,f)|^2$ for A3&A4 for ranges 16.5 km - 50 km and frequencies -500 Hz to -15 Hz.

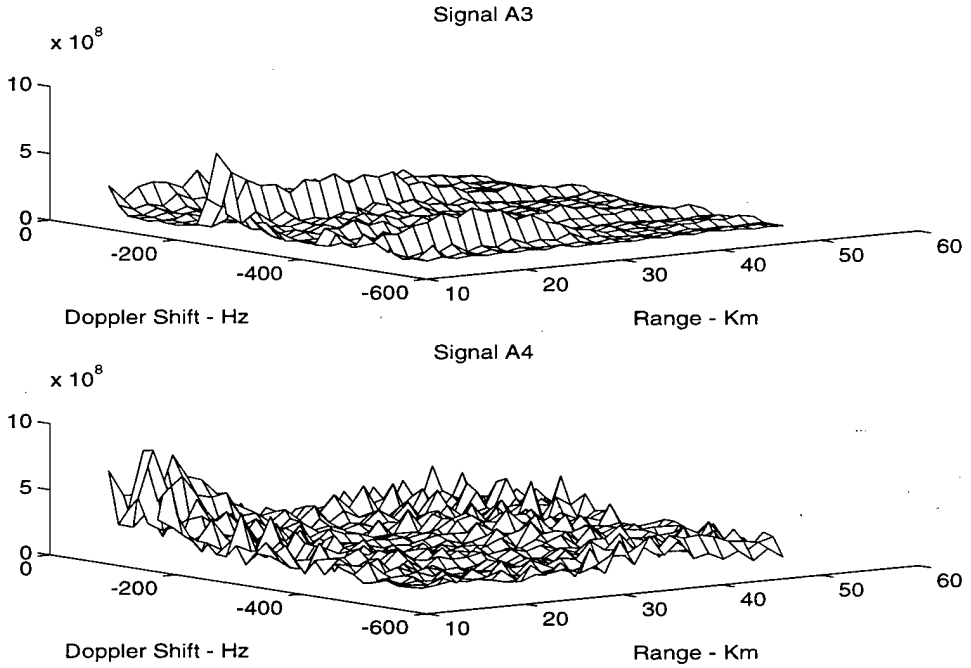

Figure 4.11: $|X(r,f)|^2$ for A3&A4 for ranges 16.5 km - 50 km and frequencies -500 Hz to -15 Hz.

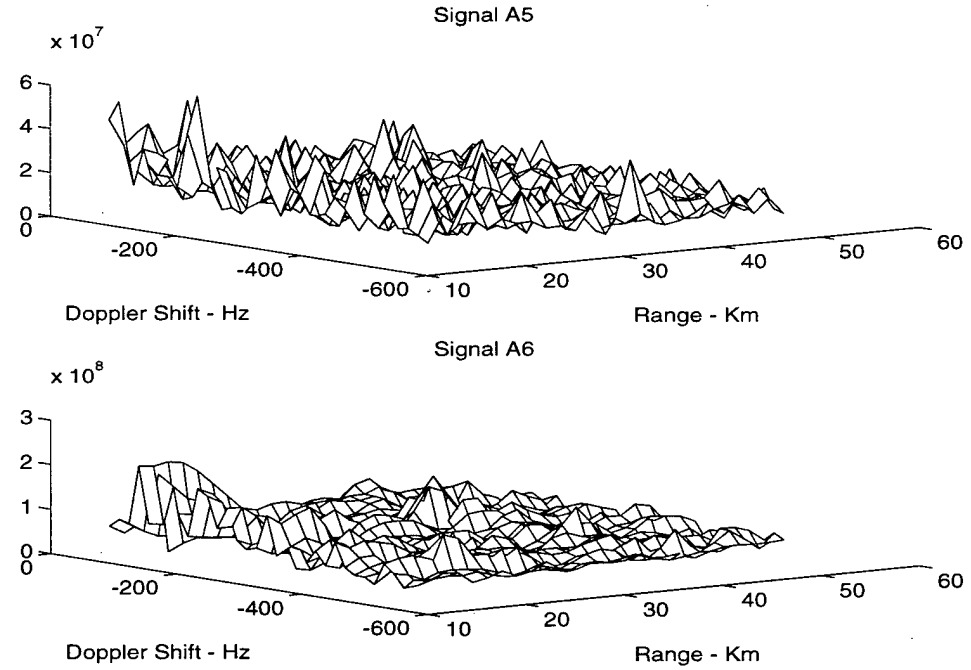

Figure 4.12: $|X(r,f)|^2$ for A5 & A6 for ranges 16.5 km - 50 km and frequencies -500 Hz to -15 Hz.

these two data sets nearly match the chi-square distribution. Indeed, when we compute the cumulative distribution and plot it versus the theoretical cumulative distribution of a χ^2_{16} A2 and A6 appear quite close to the theoretical distribution. This is shown in figure 4.14.

However, when the significance level of the Kolmogroff-Smirnoff test statistic is computed we find that it indicates that we should reject the hypothesis that the distributions are the same for all the signals.

Table 4.1: Kolmogroff-Smirnoff Statistics for A1 - A6

Signal:	A1	A2	A3	A4	A5	A6
q	0.1603	0.0429	0.3783	0.1603	0.1438	0.0795
α	$2 \cdot 10^{-18}$	0.103	$1.3 \cdot 10^{-100}$	$2.05 \cdot 10^{-18}$	$7 \cdot 10^{-15}$	$7.522 \cdot 10^{-5}$

The extremely small values of the K-S significance level definitely indicate that despite looking quite similar the distributions are indeed different. The reason for the difference is that the clutter introduces points which lie far outside the region of probability for the chi-square distribution. For example, the probability of a point being greater than 45 for the chi-square distribution is 1/7205, but we see in figure 4.13 that all the signal's histograms contain points beyond this value. This shows that this theoretical model is unable to adequately describe the characteristics of the self ambiguity function of the FM waveform. This stands even if A3 is considered an anomaly.

However, a technique does exist that can help eliminate some clutter variation at the expense of increasing the noise variance. The idea can be seen by recalling from section 3.2 that the clutter due to noise is symmetrical about the range axis in the frequency domain. There is strong evidence of this in the Figures 4.7, 4.8, and 4.9. It is also known that the target signal is a complex sinusoid and should therefore appear asymmetrically. Normally, subtracting two random variables is not advised because it increases the variance due to noise. However, in this case it is apparent that the clutter

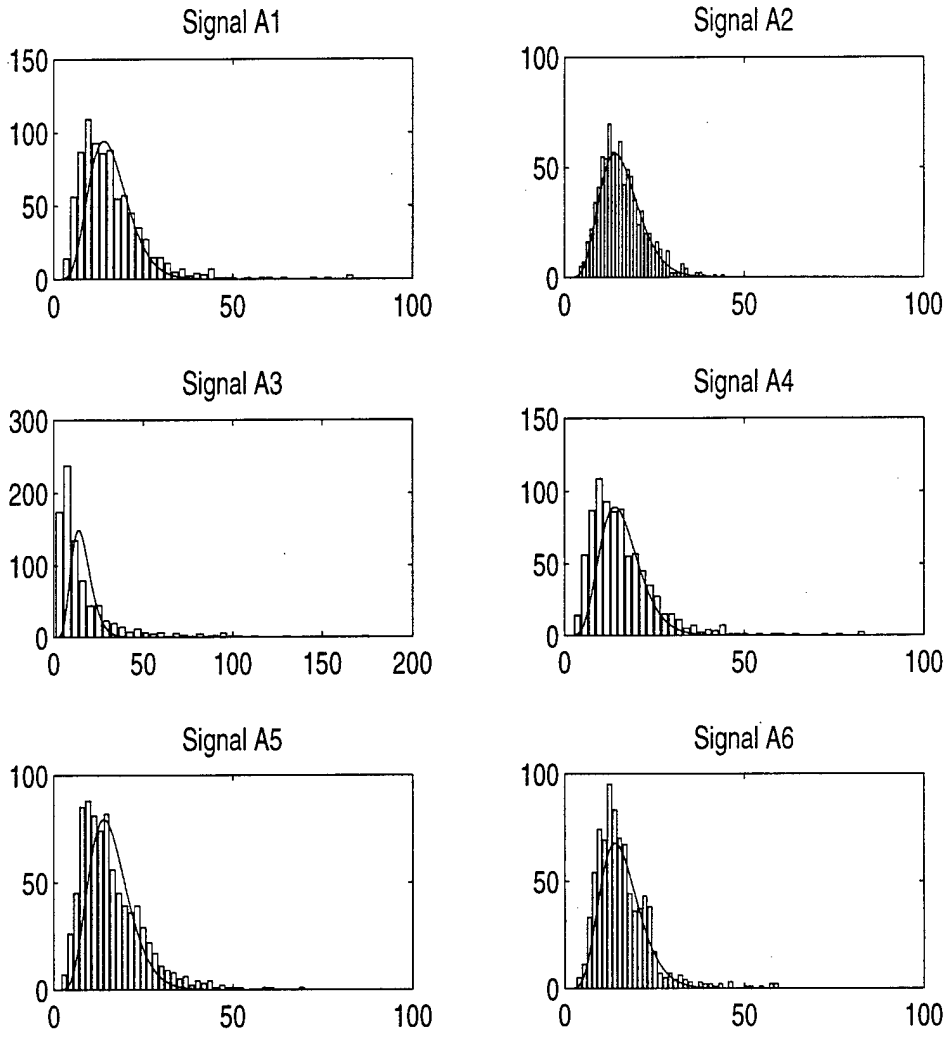

Figure 4.13: Histograms of the $|X(r,f)|^2$ for ranges 16.6-50 km and frequencies -500 Hz to -15 Hz.

contribution is dominant so the overall effect is to decrease the variance. This can be seen in the following calculation:

$$E\{(S(f)-S(-f))^2 - E\{S(f)-S(-f)\}^2\} = E\{S(f)^2\} - 2E\{S(f)S(-f)\} + E\{S(-f)^2\} - E\{S(f)\}^2 + 2E\{S(f)\}E\{S(-f)\} - E\{S(-f)\}^2 = \sigma_1^2 + \sigma_2^2 - \mathrm{cov}\{S(f),S(-f)\} \quad (4.19)$$

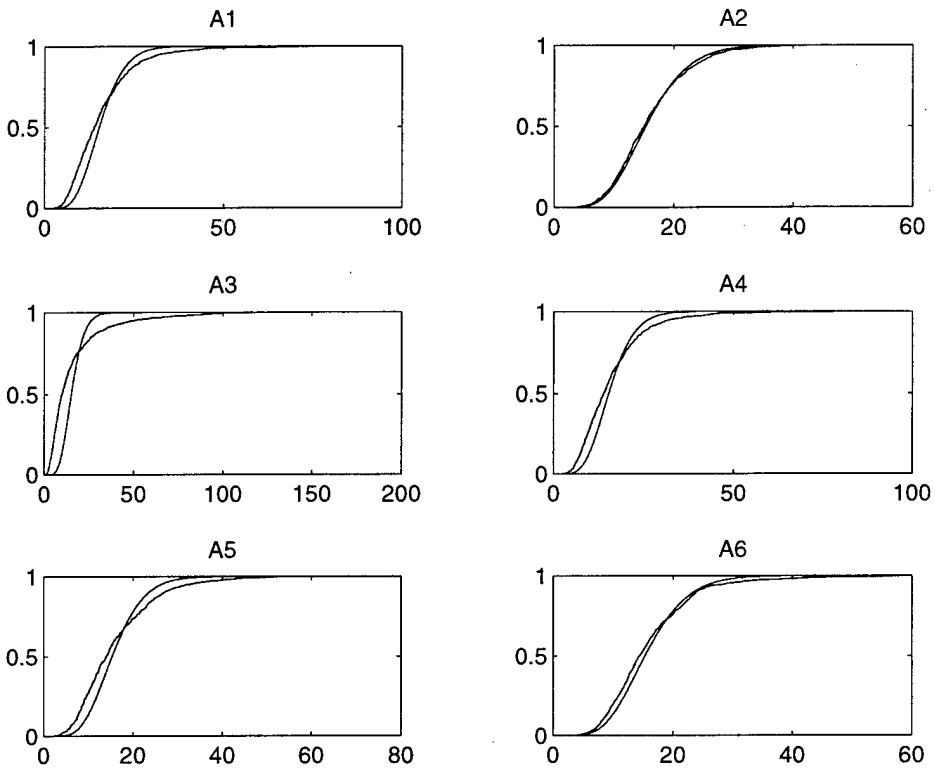

Figure 4.14: Cumulative Distribution corresponding to data and theoretical curves of figure 4.13.

where σ_1 is standard deviation of S(f) and σ_2 is the standard deviation of S(-f). Notice that if the covariance is quite large, then the overall variance of the resulting random variable is reduced.

Since the distributions are correlated, it may seem quite difficult to calculate the resulting probability density function. However, it can be shown that if we take the square root of the $|X(r,f)|^2$ then the result is a chi density of 2M degrees of freedom. Its mean, variance, and distribution are given by [10]:

$$\mu = \sqrt{2}\frac{\Gamma(\frac{2M+1}{2})}{\Gamma(M)} \qquad \sigma^2 = 2M - \mu^2 \qquad \chi_{2M} = \frac{2}{2^M \Gamma(M)} x^{2M-1} \exp(-\frac{x^2}{2}) U(x) \qquad (4.20)$$

where $\Gamma(x)$ is the gamma function and $U(x)$ is the unit step function. The chi density can be approximated by a Gaussian with mean and variance given by equation 4.20 [12]. It is well known that if two gaussian random variables are summed then even if they are correlated the result is a gaussian [10]. This means $|X(r,-f)| - |X(r,f)|$ will be a Gaussian with a mean close to zero and variance given by equation 4.19.

First, we verify that this works with the simulated data. Figure 4.15 shows the result of subtracting the positive frequencies from the negative frequencies for the white Gaussian signal. Notice that it appears to have increased the variance while making the mean near zero. Figure 4.16 shows the histogram from the data in figure 4.15 and it shows the curve representing the theoretical gaussian model with mean zero and variance given by $2\sigma^2 = 2(2M-\mu^2)$ where μ is given by equation 4.20 and M is the number of incoherent averages (M=8 in this case). Notice that the data in figure 4.15 has to be properly scaled by the square root of the factor given in equation 4.16 for the model to be applied correctly which is the reason for the different scale in figure 4.16. Next, figure 4.17 shows the plot comparing the theoretical vs. the empirical cumulative distribution. The distributions appear to nearly identical from the plot. The $\mathbf{q} = 0.0157$ which results in a significance level for the 806 points of $\alpha \approx 1$. Let's see if this procedure achieves the desired result with experimental data. Figure 4.18 shows the negative frequencies minus the positive frequencies for ranges 16.5 - 50 km for signals A1 & A2. The key fact is that the large hump is gone in A1 and that both data sets look more like identically distributed noise than in Figure 4.7. Figure 4.19 shows histograms for the negative minus positive frequency data sets for all of the experimental signals that we have looked at. Notice the definite improvement with all except A3 being closely approximated by the theoretical Gaussian curves. The parameters for the densities were estimated from the data since we already know that the normalization of equation 4.16 is not adequate for the

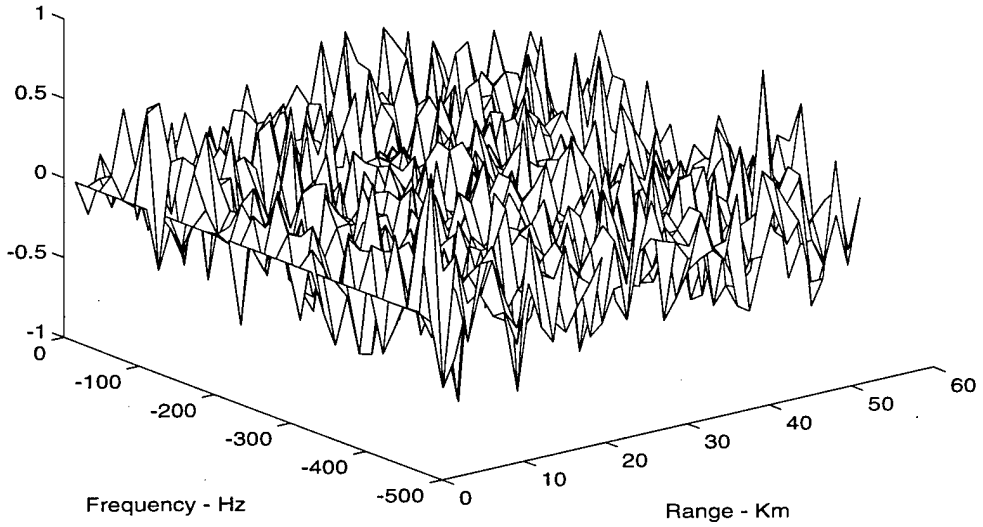

Figure 4.15: Plot of the negative frequencies minus the positive frequencies for the white Gaussian waveform.

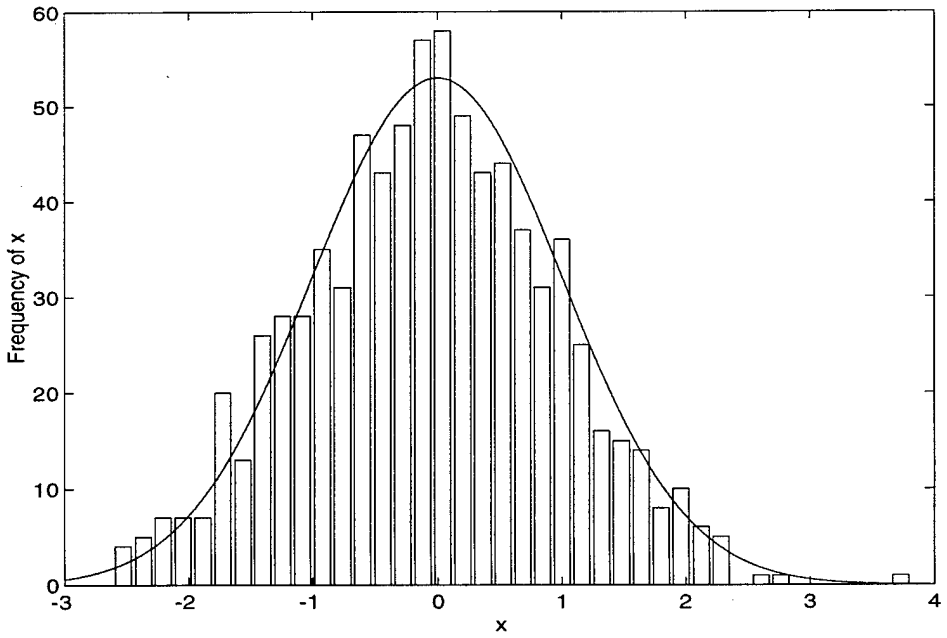

Figure 4.16: Histogram of figure 4.15 versus the theoretical Gaussian curve

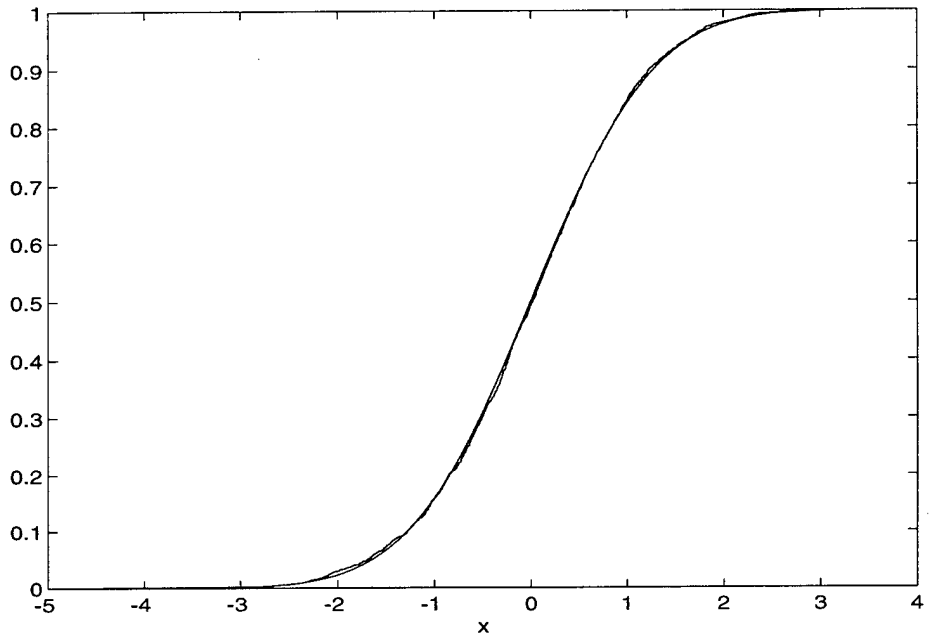

Figure 4.17: Cumulative distribution function of the theoretical (smooth curve) vs. the empirical cumulative distribution of figure 4.16.

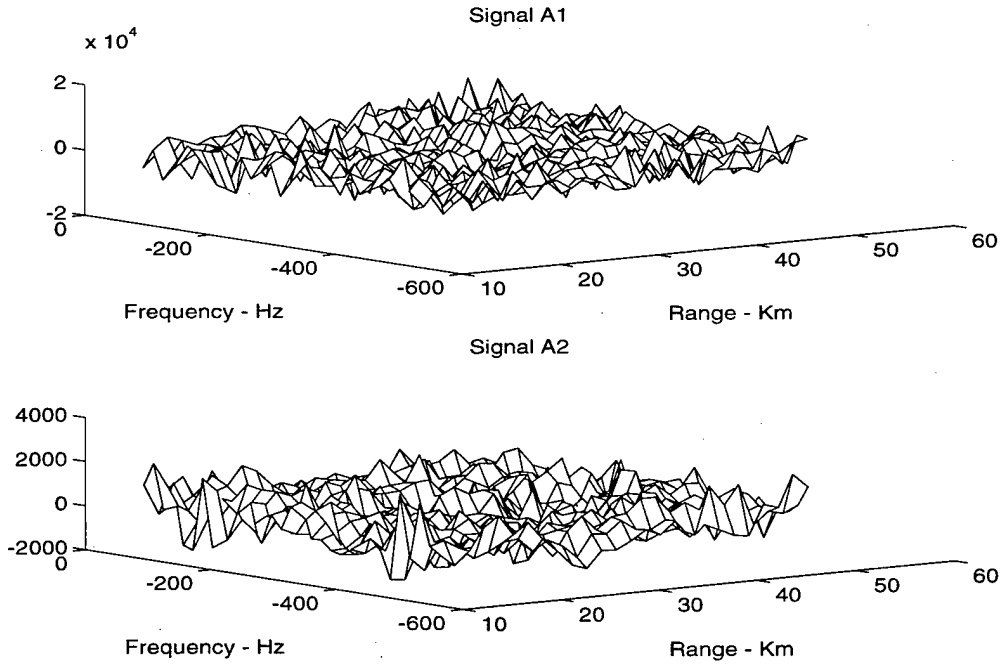

Figure 4.18: Mesh plot of |X(r,-f)| - |X(r,f)| for signals A1 & A2

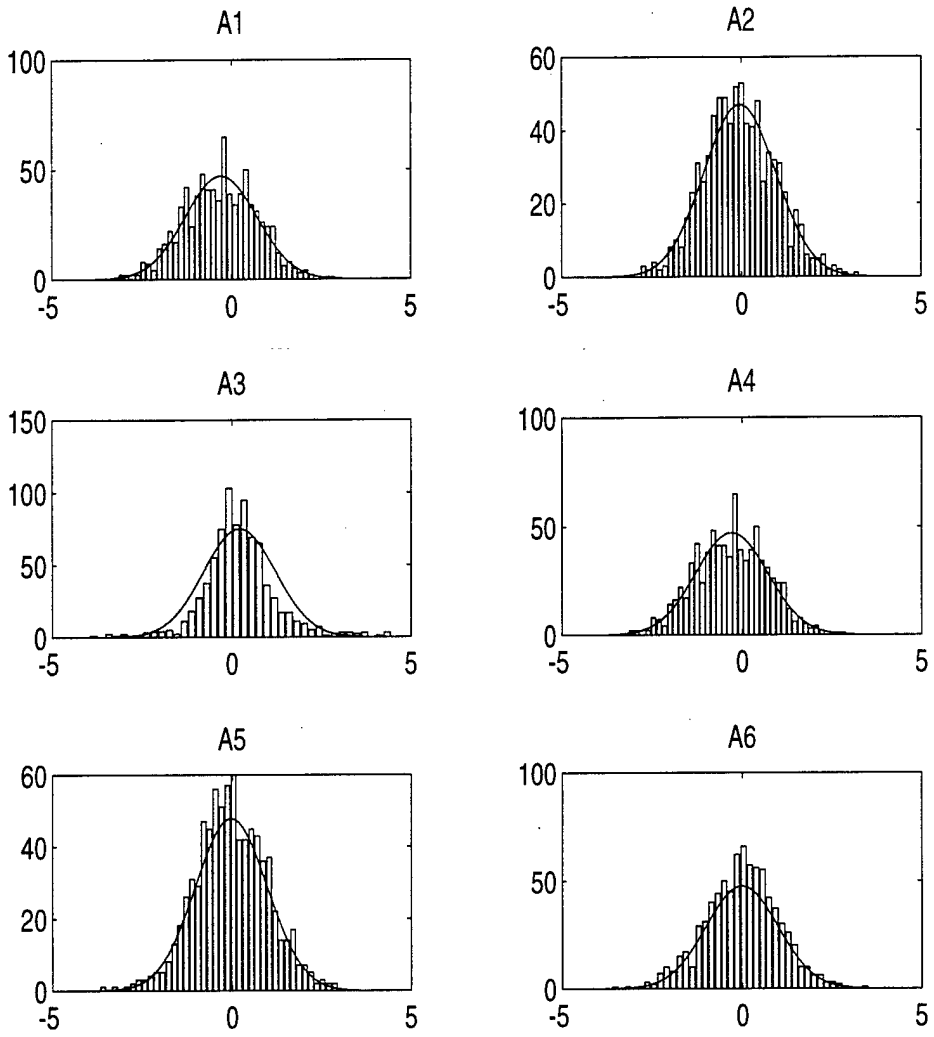

Figure 4.19: Histogram plots of |X(r,-f)| - |X(r,f)| for signals A1 - A6.

experimental data. Figure 4.20 shows the cumulative distributions that result from the histograms and the theoretical densities. Notice that all except A3 are indistinguishable from their theoretical distributions. Indeed, the K-S statistics are all close to one except for signal A3. However, the values of the significance of the K-S statistic should be taken rather heuristically since we estimated the parameters of the theoretical distribution from

Table 4.3: K-S statistics for figure 4.18

Signal	A1	A2	A3	A4	A5	A6
q	0.0266	0.0309	0.0791	0.0266	0.0221	0.0238
α	0.639	0.429	8.33E-5	0.639	0.910	0.803

the data. This seems to indicate that the distributions are close to being Gaussian. Also, the histograms of figure 4.19 show that the histograms of the data are quite similar to that of the simulated white Gaussian signal. For these reasons, and because the Gaussian distribution is simple to calculate we use it as the basis for establishing the detection threshold.

4.2 DETERMINATION OF THE DENSITY WITH A TARGET PRESENT

The next step is to determine the distribution of $|X(r,f)|^2$ when a target is present at a given range and doppler frequency. In the case of high SNR, the value of $|X(r,f)|^2$ is relatively easy to compute for a single target. First, we rewrite the signal, x(t), as $x(t) = u(t) + \alpha \exp(j2\pi\upsilon t)u(t - r_0)$. This means a(t) becomes more complex. However, as long as $r \neq r_0$ the probability density of the clutter floor remains quite similar to equation 4.16 with only the variance changing. Now when $r = r_0$ and we assume the energy of the scattered signal is much larger than the variance of the clutter floor of the ambiguity function it is possible to approximate value of the ambiguity function at r_0. This assumption allows us to write the ambiguity function at the point of the target as:

$$\left|X(r_o,\upsilon)\right|^2 \approx \left|\sum_{t=0}^{N-1} \alpha \left|u(t-r_o)\right|^2 \exp(-j2\pi t(\upsilon - f\ /\ N))\right|^2 \qquad (4.21)$$

which evaluates to $4\alpha^2\sigma^4N^2$ if $\nu \approx f/N$. Next, this value must be scaled by the quantity given in equation 4.16. The result is $2\alpha^2NMS$. However, we recognize that NMS as the length of the sequence. We rewrite this as $NMS = Tf_s$ where T is the time length in seconds and

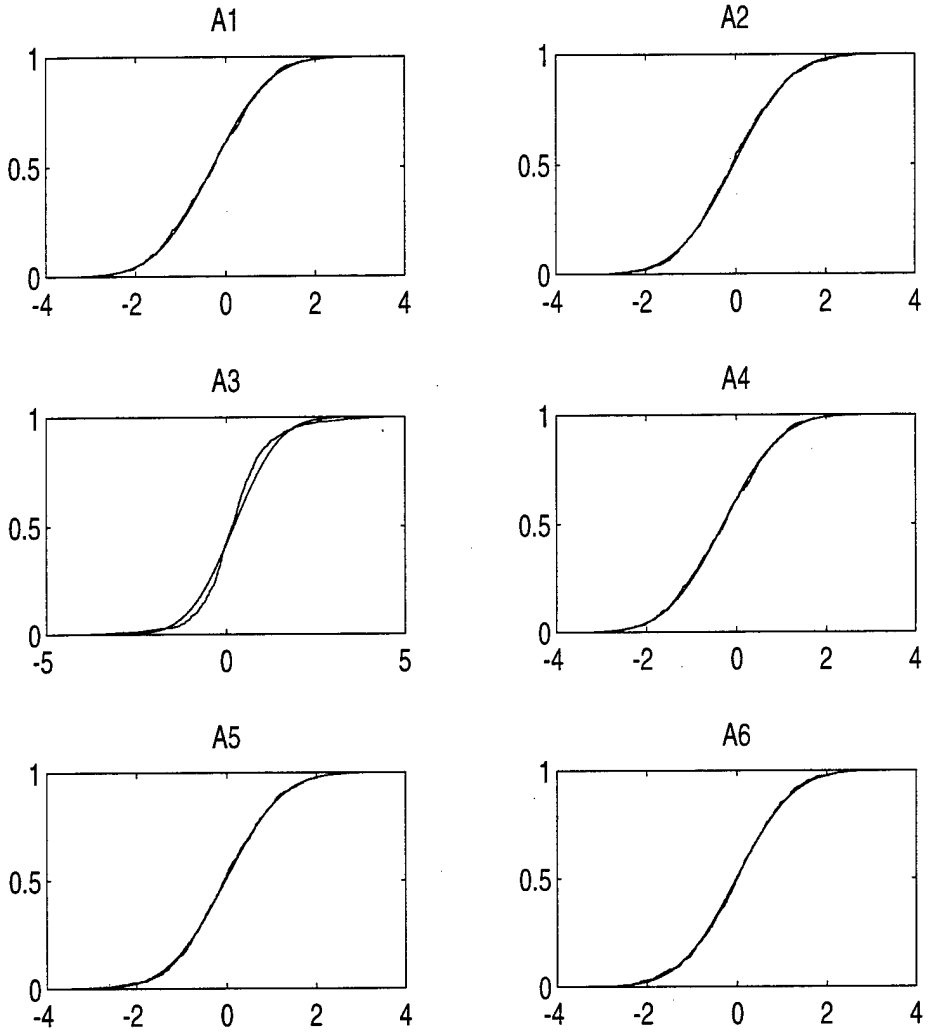

Figure 4.20: Cumulative distributions corresponding to figure 4.19.

f_s is the sampling frequency. We will call this the time-bandwidth product of the signal processing algorithm, Λ_s. Now in the case of a white noise signal the time-bandwidth product of the signal processing algorithm is equal to that of the transmitted signal, Λ_T. This means that for a white noise signal the value of the self-ambiguity function when a target is present is the ratio of the energy of the scattered signal to the power per hertz, $N_C = P_t/f_s$, of the direct signal, $2E_s/N_C$. This shows that there are two basic ways to increase the sensitivity of the radar. The first is to increase the averaging time. The second is to

increase the bandwidth of the transmitted signal. In fact, it will soon be shown that the time-bandwidth product of the FM broadcast signal is insufficient to realize the gain required to detect aircraft.

To show this for the bistatic FM radar we compute an approximate form of the probability density of $|X(r,f)|^2$ when a target is present. To do this we reconsider equation 4.21 and rewrite the inner term of the summation

$$\sum_{t=0}^{N-1}\left[x(t)x^*(t-r_0)\exp\left(-j2\pi t\frac{f}{N}\right)\right]=\sum_{t=0}^{N-1}\left\{\left[u(t)u^*(t-r_0)+\alpha u(t)u^*(t-2r_0)\cdot\right.\right.$$
$$\exp(-j2\pi v(t-r_0))+\alpha\exp(j2\pi vt)\left|u(t-r_0)\right|^2+\alpha^2\exp(j2\pi vt)\exp(-j2\pi v(t-r_0))\cdot$$
$$\left.\left.u(t-r_0)u^*(t-2r_0)\right]\exp\left(-j2\pi t\frac{f}{N}\right)\right\}\approx\sum_{t=0}^{N-1}\left[u(t)u^*(t-r_0)\exp\left(-j2\pi t\frac{f}{N}\right)\right]+ \tag{4.22}$$
$$\sum_{t=0}^{N-1}\left[\alpha\left|u(t-r_0)\right|^2\right]=A(f)+2\alpha\sigma^2N+jB(f)$$

where A(f) and B(f) are given by equation 4.7. It has been assumed here that the scattering amplitude is sufficiently small that the variance of A(f) and B(f) is not affected by the extra terms involving α. Now when we square the real and imaginary parts the result is a noncentral chi-square density [2]. The noncentral chi-square density is defined as the distribution that describes the random variable:

$$y=\sum_{n=1}^{N}\left(C_n+x_n\right)^2 \qquad \Omega=\sum_{n=1}^{N}C_n^2 \tag{4.23}$$

where the x_n are independent zero-mean Gaussian variables with common variance σ^2. The C_n are the constants and we have also defined the quantity Ω which is the parameter along with σ and N which characterize the distribution of y given in the unnormalized form as:

$$f(y)=\frac{1}{2\sigma^2}\left(\frac{y}{\Omega}\right)^{\frac{N-2}{4}}\exp[-(y+\Omega)/(2\sigma^2)]I_{N/2-1}\left(\frac{\sqrt{\Omega y}}{\sigma^2}\right) \tag{4.24}$$

where $I_{N/2-1}(y)$ is the modified Bessel function of first kind and order N/2-1. The case of interest is the noncentral chi-square that results when the value of the square of the

ambiguity function at the range and doppler frequency of the target is computed with both coherent and incoherent integration. Coherent integration scales the variance of A(f) and B(f) as described earlier by a factor of 1/S. Incoherent integration requires that we rewrite the step as:

$$S(f) = \frac{1}{M}\sum_{i=0}^{M-1} S_i(f) = \frac{1}{M}\sum_{i=0}^{M-1}(A_i(f) + 2\alpha\sigma^2 N)^2 + \frac{1}{M}\sum_{i=0}^{M-1}\left(B_i(f)\right)^2 = \sum_{i=0}^{M-1}\left(\frac{A_i(f)}{\sqrt{M}} + \frac{2\alpha\sigma^2 N}{\sqrt{M}}\right)^2 + \sum_{i=0}^{M-1}\left(\frac{B_i(f)}{\sqrt{M}}\right)^2 \tag{4.25}$$

This means the variance is $\sigma_S^2 = 2\sigma^4 N/MS$ and that $\Omega = 4\alpha^2\sigma^4 N^2$. Next we normalize the S(f) by its variance (notice it is the same as the normalization parameter in 4.16). This results in the normalized noncentral chi-square distribution with noncentrality parameter $\lambda = \Omega/\sigma_S^2 = 2\alpha^2 NMS = 2\alpha^2\Lambda_S$. This results in the standard form of the noncentral chi-square density with noncentrality parameter λ [2]:

$$\begin{aligned} f(y) &= \frac{1}{2}(y/\lambda)^{(2M-2)/4}\exp(-(y+\lambda)/2) I_{M-1}(\sqrt{\lambda y}) \\ \mu_y &= \lambda + 2M \\ \sigma_y^2 &= 4\lambda + 4M \end{aligned} \tag{4.26}$$

where N has been substituted by 2M because we summed 2M independent noncentral chi-square densities. Figure 4.21 is a plot of the normalized noncentral chi-square density with α=0.02, N = 64, M = 8, and S = 250 contrasted with the chi-square density of 2M degrees of freedom. Notice that there is almost no overlap between the densities which means probability of detection, $P_D \approx 1$, and probability of false alarm, $P_{FA} \approx 1$. Next, we consider the density of the modulus of the ambiguity function, |X(r,f)|, at the target. The

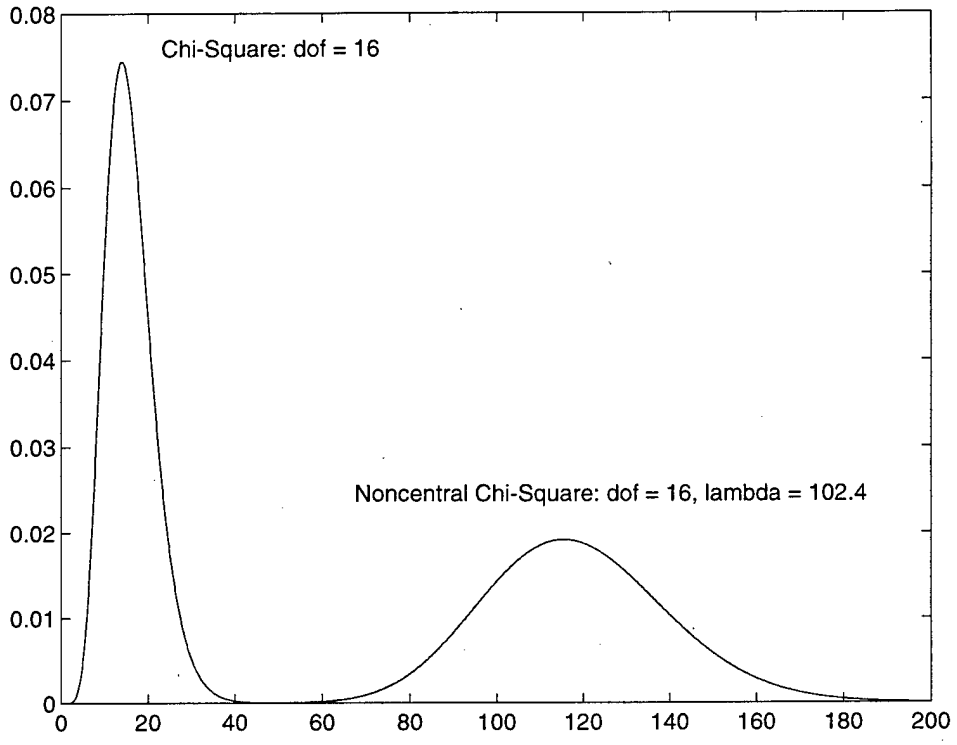

Figure 4.21: Plot of noncentral chi-square with λ=102.4, 2M = 16, versus a chi-square of 2M = 16 degrees of freedom.

density is simply the noncentral chi density given by [2]:

$$f(y) = y\left(\frac{y^2}{\lambda}\right)^{\left(\frac{2M-2}{4}\right)} \exp\left(-\frac{\lambda}{2}-\frac{y^2}{2}\right) I_{M-1}\left(\sqrt{y^2\lambda}\right) \tag{4.27}$$

where λ is the same noncentrality parameter as before and $I_{M-1}(y)$ is still the modified Bessel function of the first kind. The mean and variance of the noncentral chi density can be approximated as [from equation 26.4.38 found in reference 12]:

$$\mu = \sqrt{a - \frac{(1+b)}{2}} + O(a^{-3/2}) \qquad a = \lambda + 2M \qquad b = \lambda / a$$
$$\sigma^2 = \left(\frac{1+b}{2}\right) - \frac{1}{8a}[8b + (1+b)(1-7b)] + O(a^{-2}) \tag{4.28}$$

However, if the noncentrality parameter is moderately greater than the degrees of freedom, 2M, then we may take b≈1. This means we can approximate the mean as $\mu \approx \sqrt{\lambda + 2M - 1}$ and $\sigma^2 \approx 1$. Although, first order correction could be completely made this will be quite close if the condition above is met (this will be the case for any targets we wish to detect because the mean must be greater than the mean of the clutter). In addition this approximation lowers the estimate of the mean and increases the value of the variance. This is good because it means the true values will yield a better probability of detection than the approximation will.

Because the chi density can be approximated as Gaussian, it follows that the noncentral chi density can be approximated as the Gaussian density, $N(\sqrt{\lambda + 2M - 1}, 1)$. This means that when the positive frequencies are subtracted from the negative frequencies that if a target is present its distribution is given as a Gaussian with mean and variance of:

$$\mu = \sqrt{\lambda + 2M - 1} - \sqrt{2}\frac{\Gamma\left(\frac{2M+1}{2}\right)}{\Gamma(M)} \qquad \sigma^2 = 1 + 2M - \left(\sqrt{2}\frac{\Gamma\left(\frac{2M+1}{2}\right)}{\Gamma(M)}\right)^2 \tag{4.29}$$

However, just as the noncentral chi density's mean and variance can be approximated, we can do the same with the chi density. Abramowitz and Stegun (equation 26.4.34) give the approximations as [12]:

$$\begin{aligned} \mu &= \left\{1 + [32M(2M-1)]^{-1}\right\}\sqrt{2M - \frac{1}{2}} + O((2M)^{-7/2}) \approx \sqrt{2M} \\ \sigma^2 &= \frac{1}{2} - \frac{1}{16M} - \frac{1}{64M^2} + \frac{5}{512M^3} + O((2M)^{-4}) \approx \frac{1}{2} \end{aligned} \tag{4.30}$$

Where we have used the assumption that M>2, which means that we are overestimating the mean and variance of the clutter. This good because when subtracted from the noncentral chi density it makes the mean smaller than it should be and the variance larger.

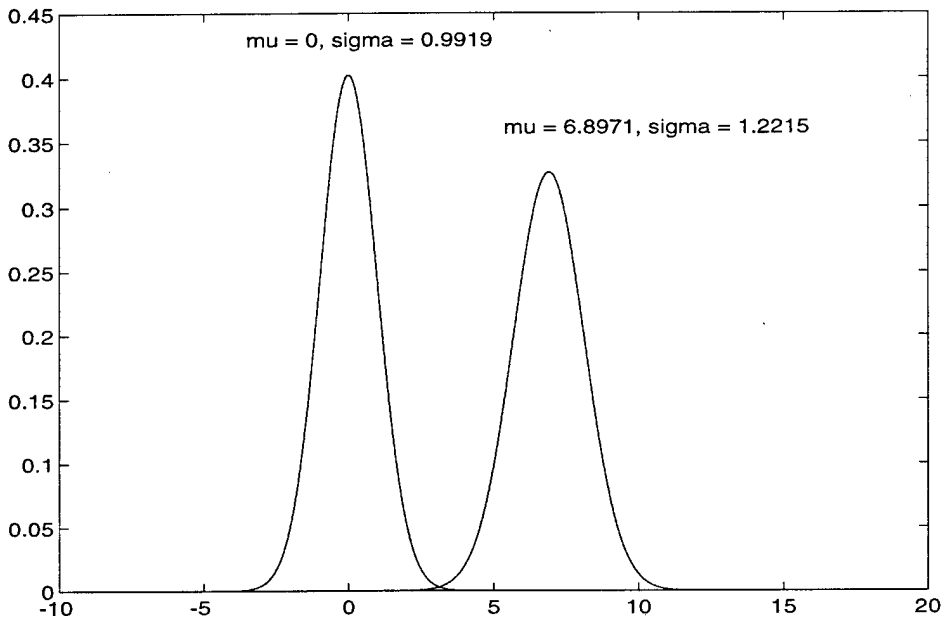

Figure 4.22: Plot of gaussian with mean ≈6.84, variance ≈1.5 versus a gaussian with mean ≈0 and variance ≈1

Thus, it will generate a probability of detection which is slightly less than the true value. Using 4.30 we may rewrite 4.29 as:

$$\mu \approx \sqrt{\lambda + 2M - 1} - \sqrt{2M} \qquad \sigma^2 \approx 1.5 \tag{4.31}$$

4.3 IDEAL OPERATING CHARACTERISTICS OF THE WHITE GAUSSIAN SIGNAL

The previous two plots give us an intuitive feel for how the operating characteristics of the radar can be determined from equations 4.16, 4.20, 4.26, and 4.29. The figures show the detection of a target can be posed as binary hypothesis-testing problem with hypotheses: H_0 - No target present and H_1 - target present. The performance of the radar is determined by finding the P_d, the probability of detection, and P_f, the probability of false alarm.

Although many possibilities exist, we choose to analyze the performance of the radar through a simple threshold system. The system is simply:

$$\left|X(r,f)\right|^2 > X_t \qquad \text{or} \qquad \left|\left|X(r,-f)\right| - \left|X(r,f)\right|\right| > X_t \tag{4.32}$$

where the second equation is a two sided threshold which allows detection of a target at either a positive or negative frequency. The probability densities that describe the first test are given by equations 4.16 and 4.26. The mean and variance of the Gaussians that describe the second test are given by 4.20 and 4.29. The probability of false alarm for the simple threshold system is given by $P_f = P\{\left|X(r,f)\right|^2 > X_t \mid H_0\}$, and the probability of detection is given by $P_d = P\{\left|X(r,f)\right|^2 > X_t \mid H_1\}$. These can be easily determined after X_t is chosen by integration of the appropriate probability density. However, in radar it is desirable to chose a maximum value of P_f and then to choose the threshold level to maximize P_d which is called the Neyman-Pearson strategy [2]. In this case, it is obvious that the threshold value(s) that will achieve this can be determined either from the percentage points of a chi-square or the standard deviation of a Gaussian.

First, we consider the performance characteristics using the square of the ambiguity function. The distribution when no target is present is the χ^2_{2M} and with a target it is the noncentral chi-square of equation 4.26. Figure 4.23 is the plot of the P_d vs. P_f with values of 20log(α), the ratio of the scattered signal's power to the direct signal, given in the plot. Notice that for values of 20log(α) < -38 dB that detection with a reasonable value for P_f is unlikely for the given values of M, N, and S. A good question to ask is how does changing M, N, or S affect the probability of detection. First, we notice that changing N or S does not change the density of H_0, however, changing M increases the mean and variance of the χ^2_{2M} which is the density of H_0. The effect of increasing the values N and S for the noncentral chi-square can be seen

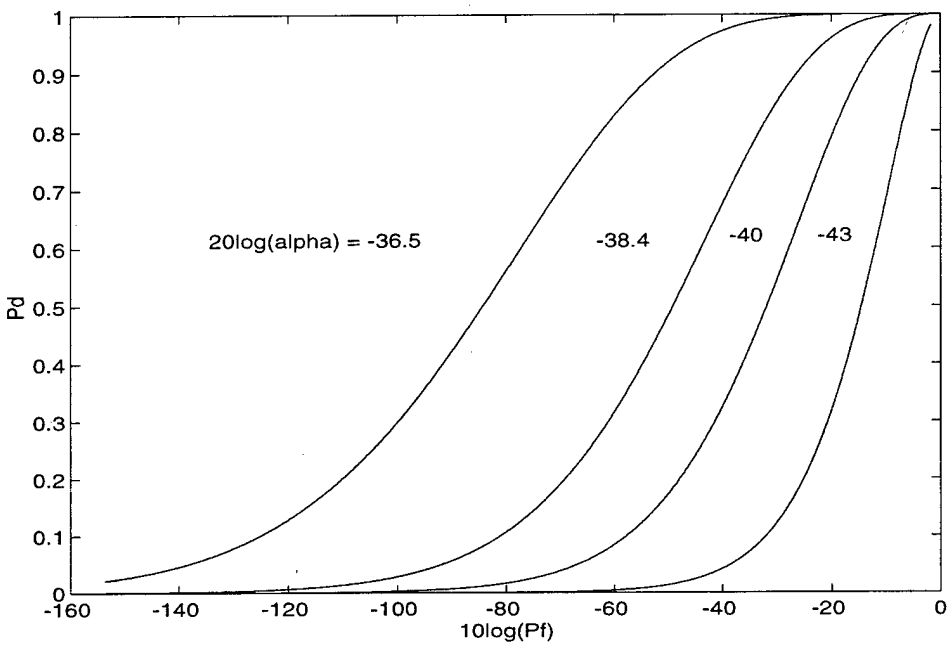

Figure 4.23: P_d vs. P_f for the White Gaussian Signal with M = 8, N = 64, S = 250, and 20log(α).

to directly increase the noncentrality parameter $\lambda = 2\alpha^2NMS$. Notice that the sampling frequency, f_s, divided by NS gives the frequency resolution of the ambiguity function. If we keep the same frequency resolution, then any changes of N or S which are governed by the equation $NS = f_s$ will not change the probability of detection. Now the length of the time series from which we generate the ambiguity function is NMS. This means for a constant time-bandwidth product the only interesting tradeoff to investigate is between N or S and M. It is obvious that since the time-bandwidth product is constant that it is ideal to pick M as small as possible because this will decrease the variance of the clutter. Figure 4.24 shows this for $\Lambda_s = 128{,}000$, and $P_f = 10^{-6}$.

Next, we determine the performance characteristics for the threshold described by the second equation of 4.29. Notice that it requires a two sided threshold. However, because of the symmetry of the gaussian random variable we only consider the one sided case of the target being located at a negative frequency. This test requires that

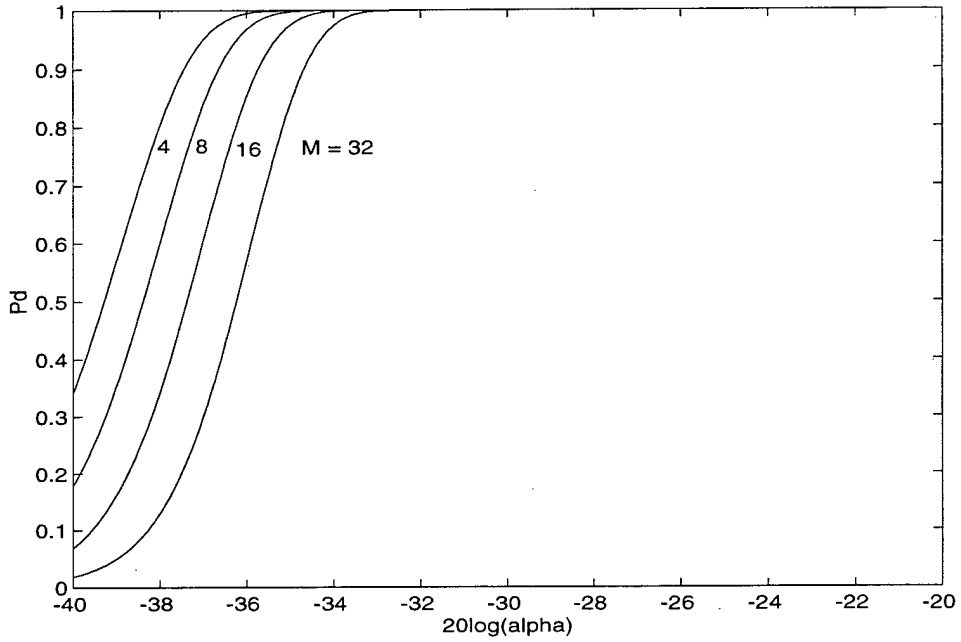

Figure 4.24: Plot of P_d vs. α for constant $P_f = 10^{-6}$ and $\Lambda_s = 128{,}000$. M is indicated on the plot.

M>2 because of the approximation of the chi density by a Gaussian. However, it is useful for two reasons. First, the Gaussian probability density is simple to work with especially in determining the P_f. Second, section 4.1.2 showed that the actual FM radio data appeared to be more accurately characterized by a Gaussian density if the frequencies were subtracted. Figure 4.25 shows the same plot as figure 4.22 except the densities are now Gaussians with means and variances described by equations 4.26 and 4.29. It is useful to determine a formula which can be used to determine the minimum detectable scattered signal as a function of P_f, P_d, M, N, and S. This task can be accomplished by considering the two Gaussian densities. First we set the false alarm rate by setting the threshold level at a multiple of the standard deviation of the density that corresponds to no target present. Next, we set the minimum probability of detection by subtracting a multiple of the standard deviation from the mean of the distribution corresponding to the target. We then

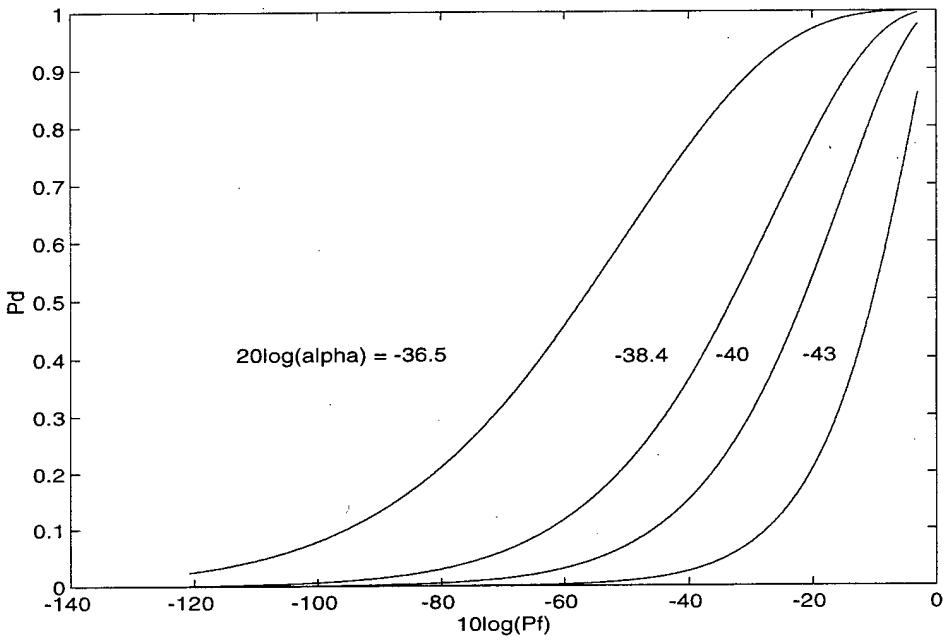

Figure 4.25: P_d vs. P_f for the White Gaussian Signal with M = 8, N = 64, S = 250, and 20log(α).

equate the results. This results in:

$$\mu - n\sigma' = k\sigma \tag{4.33}$$

where μ and σ′ are given by equation 4.31 and σ is approximated as one from equation 4.30. We can then substitute these values into 4.33 which gives the following result:

$$\lambda = 1 + 3.464n\sqrt{M} + 2.828k\sqrt{M} + 1.5n^2 + 2.449nk + k^2 \tag{4.34}$$

However, we may rewrite $\lambda = 2\alpha^2 NMS = 2\alpha^2\Lambda_s$. This means we can now solve for the minimum scattering amplitude that is detectable as:

$$\text{M>2} \qquad \alpha_{\min}^2 = \frac{1 + 3.464n\sqrt{M} + 2.828k\sqrt{M} + 1.5n^2 + 2.449nk + k^2}{2\Lambda_S} \tag{4.35}$$

The probability of detection is given by $P_d = \text{erf}(x)+0.5$ and the probability of false alarm is given by $P_f = 0.5 - \text{erf}(k)$ where we are using the definition [10]:

$$\text{erf}(x) = \frac{1}{\sqrt{2\pi}} \int_0^x \exp(\frac{-y^2}{2}) dy \qquad (4.36)$$

The following table shows how the minimum detectable scattering amplitude decreases as the observation time increases for a single target:

Table 4.4: Minimum detectable scattering amplitude for WG sampled at 250 kHz

T (seconds)	M	P_d	P_f	$20\log(\alpha_{min})$
0.5	8	0.841	10^{-6}	-34.71
0.5	4	0.841	10^{-6}	-35.50
1	16	0.841	10^{-6}	-36.808
1	4	0.841	10^{-6}	-38.51
2	32	0.841	10^{-6}	-38.79
2	4	0.841	10^{-6}	-41.52
4	64	0.841	10^{-6}	-40.66
4	4	0.841	10^{-6}	-43.742
8	4	0.841	10^{-6}	-46.75
16	4	0.841	10^{-6}	-50.6

Notice doubling the observation time T doubles the sensitivity of the radar because it doubles the time-bandwidth product when no change in the number of incoherent averages occurs. This is what we would expect because this doubles the energy of the scattered signal while the increase in NS appropriately scales the clutter power to keep its contribution constant. This table also indicates that even at a bandwidth of 250 kHz that the time length of the series must extremely long in order for the SDRs of -60 dB to be detected.

4.3 ADJUSTMENTS FOR THE FM WAVEFORM

The previous section discussed the ideal operating characteristics for a radar with a white Gaussian signal with no clutter besides itself and a single scattered signal. Unfortunately, this is not an ideal world and neither the signal of interest, FM broadcasts, is not a white Gaussian process and of course there are buildings, cars, and the earth all of which introduce clutter into the detection problem. Finally, there are receiver noise sources which will also increase the variance of the clutter floor. In this section we discuss how the non-ideal world effects our calculations and we propose a crude phenomenological correction to our equations which should allow order of magnitude estimates to be made.

The non-ideal factors of the FM broadcast can be broken into three categories:

1) The FM broadcast is not White Gaussian noise. However, the Central Limit Theorem can still be applied because over time intervals longer than approximately 20 microseconds the data is uncorrelated. The difference is that the calculation of the variance must be modified to account for correlation. This can also be viewed as bandwidth inefficiency. If the broadcast were sampled at a slower rate of 30 kHz, then it would be much closer to being a white process.

2) The FM broadcast is not just the direct broadcast but also includes scatter from the earth, buildings, and cars as well as the airplane we are interested in. This scatter will be mostly concentrated near zero range so it should not introduce much bias. However, it will increase the overall variance of the process.

3) The target of interest is an aircraft and in general is moving (possibly accelerating). This means the scattering amplitude is best modeled as a Rayleigh random variable with uniformly distributed phase [8].

First, we examine the increase in variance due to using a signal with nonzero correlation for lags other than zero. It can easily be shown that the variance of the sum of two random variables which are correlated can be given as:

$$E\{(x+y)^2\} = E\{x^2\} + 2E\{xy\} + E\{y^2\} = \sigma_x^2 + 2r\sigma_x\sigma_y + \sigma_y^2 = 2\sigma^2(1+r) \tag{4.37}$$

where r, the correlation coefficient, can be inferred from 4.37 and is between 0 and 1. The correlation this introduces can be represented as follows:

$$\sigma_S^2 = \frac{2\sigma^4 N}{MS} + \gamma = \frac{2N}{MS}(\sigma^4 + \frac{MS}{2N}\gamma) = \frac{2N}{MS}\sigma_r^4 \tag{4.38}$$

where σ_r^4 is the rescaled value of the semivariance of the signal. Notice that this can also be expanded to include the increase in variance due to physical clutter such as buildings, cars, ect. This does not change the value of Ω that is generated by equation 4.25. This means that these two effects can be accounted for by adjusting the noncentrality parameter as follows:

$$\lambda = \Omega / \sigma_r^4 = 2\alpha^2 \Lambda_S (\sigma_t^4 / \sigma_r^4) = 2\alpha^2 \Lambda_S \beta \tag{4.39}$$

where β is the ratio of the true transmitted signal's variance, σ_t^2, to the rescaled variance given by 4.38. We suggest here that it is best to empirically determine β from repeated observations of radio broadcasts. We can do this in two parts. First, we approximate the increase in the semivariance caused by the clutter. This can be done by using a directional antenna or adaptive beamforming to isolate the scattered signals. Then the semivariance due to physical clutter only can be estimated. This can then be added to the direct signal's variance to give σ in equation 4.38. Another way is to use a worst case scenario estimate for the physical clutter.

Now we can estimate the ratio $\hat{\beta} = \frac{\sigma^4}{\sigma_r^4} = \beta(1+\xi)^2$ where ξ represents the ratio of the physical clutter to the broadcast signal's variance. Next we use the linearity of the expectation operator to determine $\hat{\beta}$. We do this by first estimating σ^2 from either

the real or imaginary component of the complex data. Then we use this estimate to scale the ambiguity function by equation 4.16. Here it is now possible to estimate $\hat{\beta}$ either from the mean of the chi-square distribution or from the variance of the Gaussian density which is empirically generated from the clutter floor. This means we have:

$$\hat{\beta} = \frac{\hat{\mu}_{\chi^2_{2M}}}{2M} = \frac{\hat{\sigma}_N^2}{2(2M - \mu_N^2)} \Rightarrow \beta \approx \frac{\hat{\beta}}{(1+\xi)^2} \tag{4.40}$$

The following table lists the estimates for $\hat{\beta}$ of signals A1 - A6 for Λ_s= 128,000 and M = 8.

Table 4.5: List of $\hat{\beta}$, the bandwidth inefficiency factor, for signals A1-A6

Signal	$\hat{\beta}$
A1	0.12
A2	0.16
A3	0.07
A4	0.12
A5	0.23
A6	0.22
Average	0.15

This suggests $\hat{\beta}$ is probably close to 0.15 and that if we take a conservative value of ξ = 0.5 this shows that β is close to 0.067. It is interesting to note that the ratio of the true bandwidth occupied by the signal, 30 kHz, to the sampling frequency, 250 kHz, is 0.12. This seems to indicate that $\hat{\beta}$ is a parameter which determines bandwidth inefficiency. This value can now be used to estimate the corrected value of the noncentrality parameter. No change occurs to the chi-square and chi densities of the clutter. Figure 4.26 shows the P_d vs. P_f for the same case as 4.24 except the noncentrality parameter is corrected for the value of β=0.067.

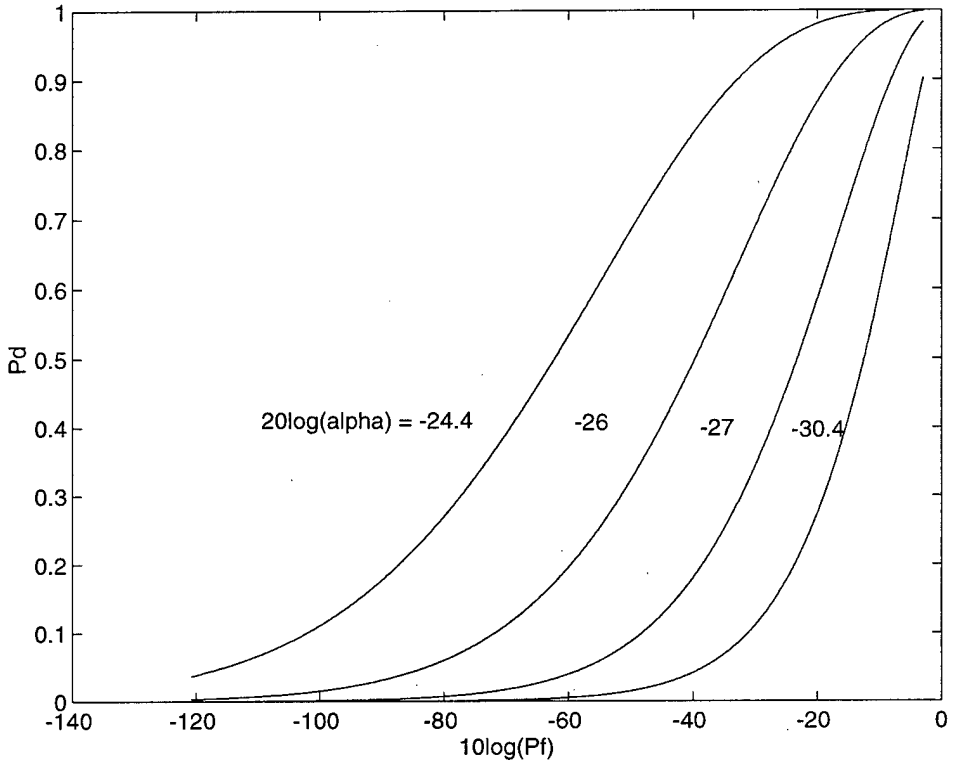

Figure 4.26: P_d vs. P_f for T = 0.5 seconds and M = 8 with β=0.067.

The correction to λ means that equation 4.35 is:

$$\text{M>2} \qquad \alpha_{\min}^2 = \frac{1 + 3.464n\sqrt{M} + 2.828k\sqrt{M} + 1.5n^2 + 2.449nk + k^2}{2\Lambda_S \beta} \tag{4.41}$$

The results for β=0.067 appear in table 4.6 on the following page. From this table, it appears that it would be possible to detect a target whose power relative to the direct signal is -38.8 dB. However, we must recall that the aircraft will move over 4 km during this time period and could change its velocity by 157 m/s if its limited to a one g maneuver. This means table 4.6 and equation 4.41 should still only be taken as lower bounds for the minimum detectable scattered signal.

Table 4.6: Minimum detectable scattering amplitude for FM signal sampled @ 250 kHz

T (seconds)	M	P_d	P_f	$20\log(\alpha_{min})$
0.5	8	0.841	10^{-6}	-23.0
0.5	4	0.841	10^{-6}	-23.8
1	16	0.841	10^{-6}	-25.1
1	4	0.841	10^{-6}	-26.8
2	32	0.841	10^{-6}	-27.1
2	4	0.841	10^{-6}	-29.8
4	64	0.841	10^{-6}	-28.9
4	4	0.841	10^{-6}	-32.8
8	4	0.841	10^{-6}	-35.8
16	4	0.841	10^{-6}	-38.8

However, there exist multi-threshold tracking algorithms that could possibly be used to approach this lower bound. Also, for short time periods table 4.6 should be close to the real situation because most aircraft are limited in velocity and acceleration.

Figure 4.27 is a plot of the minimum detectable signal for the white gaussian signal where the plot is $|X(r,-f)|-|X(r,f)|$ with a target located at 21 km and -125 Hz (a fourier frequency). The length of the time series was 0.512 s with $P_f = 10^{-5}$ and $P_d = 0.5$. Figure 4.28 is the plot of $|X(r,f)|^2$ for the same signal which shows that is important to have the statistics in mind when making judgments about detectability. Figure 4.29 is the plot of signal A3 with an computer generated scattered signal injected at the level of minimum detectability, $P_d = 0.645$ and $P_d = 10^{-5}$ where we have taken $\beta=0.15$. Figure 4.30 is signal A3 with a scattered signal whose SDR, α^2, is 3 dB below the signal injected to make figure 4.27.

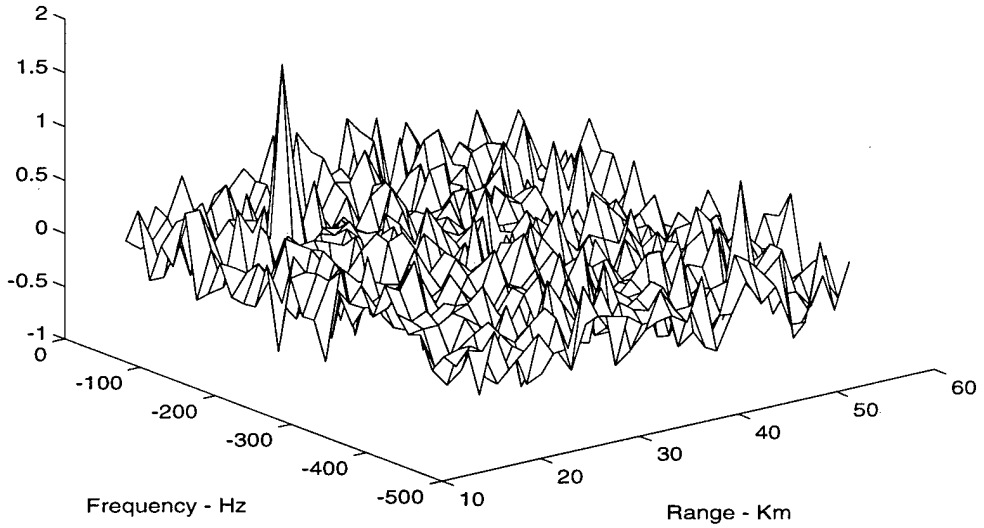

Figure 4.27: Plot of $|X(r,-f)|-|X(r,f)|$ for Λ_s = 128,000, M=8, $P_f = 10^{-5}$, and P_d = 0.5 for a white gaussian signal with target at 21 km and -125 Hz.

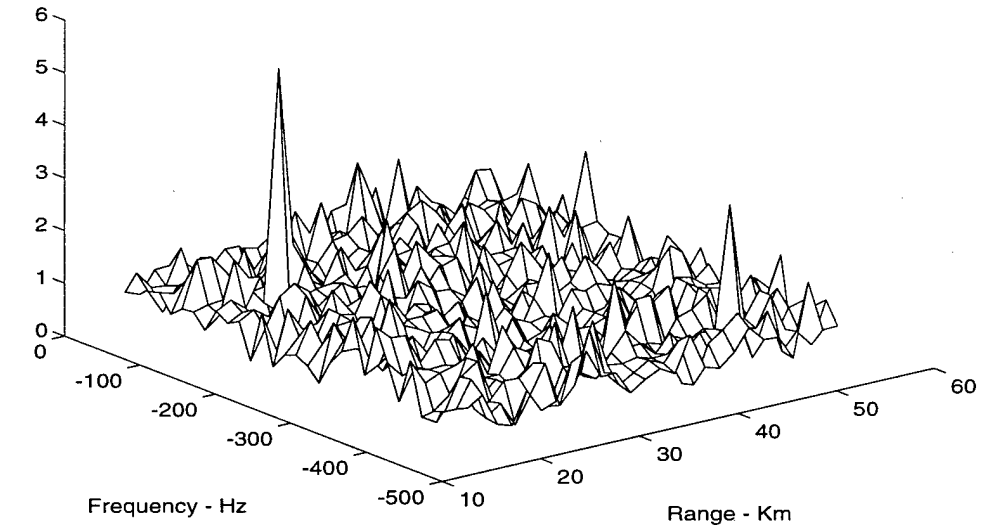

Figure 4.28: Plot of $|X(r,f)|^2$ for Λ_s = 128,000, M=8, $P_f = 10^{-5}$, and P_d = 0.5 for a white gaussian signal with target at 21 km and -125 Hz.

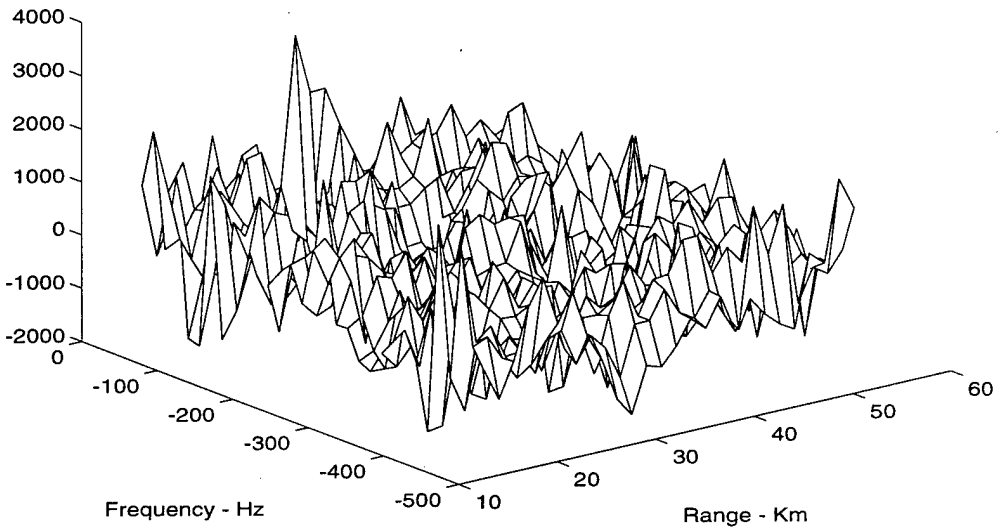

Figure 4.29: Plot of |X(r,-f)|-|X(r,f)| for Λ_s = 128,000, M=8, $P_f = 10^{-5}$, β=0.15 and P_d = 0.645 for signal A2 with target at 21 km and -125 Hz.

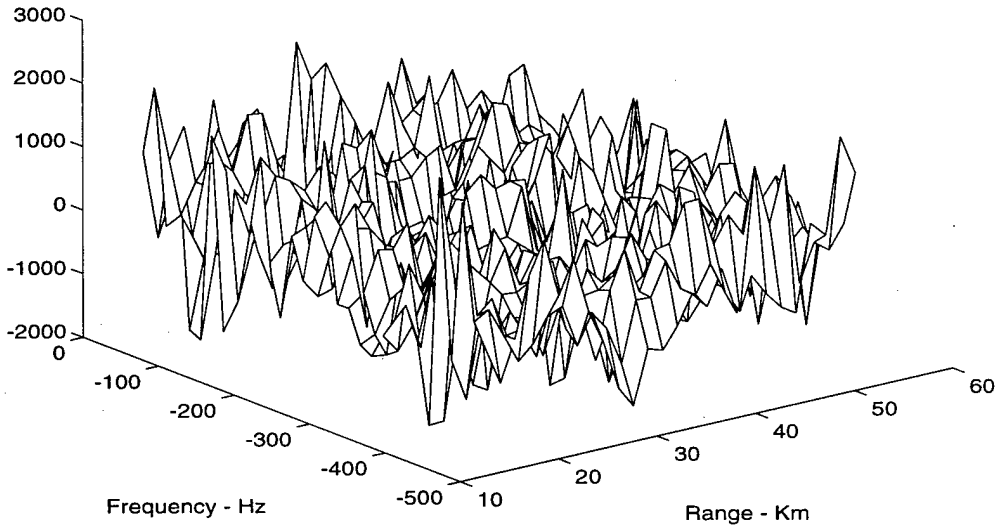

Figure 4.30: Same as figure 4.29 except α was decreased by 3 dB.

CHAPTER 5: ADAPTIVE BEAMFORMING/DIRECTIONAL ANTENNAS

The last chapter discussed the limitations of the monostatic FM radar with one receiver. It is obvious that isolating the scattered signal from the direct broadcast signal should improve the sensitivity of the radar. Indeed, this is the impetus for using the Cascade Mountains as a barrier to shield the receiver at Manastash Ridge from the direct FM broadcast. However, it is possible to eliminate through spatial isolation the direct signal without having to use two receivers which are physically separated by a barrier. This can be done either through using antennas with directional gains or a number of omnidirectional dipoles whose signals are phase shifted and then summed. In the case of dipoles, the phase shifting can adapt over time to provide a time-varying optimal response to the radio environment. Hence, the name adaptive beamforming. However, this differs from the use of a physical barrier because a physical barrier will also attenuate random scatter of the direct signal by buildings, cars, and the earth. The question of interest is how does physical clutter limit a directional antenna/adaptive beamforming monostatic FM radar. We will limit our discussion to adaptive beamforming because limited experimental data was available to explore this option. Also, the results of using directional antennas should be quite similar.

5.1 SYSTEM OVERVIEW

The basic idea of adaptive beamforming can be seen in figure 5.1. An array of more than one antenna is arranged in linear fashion which causes the phase shift of the incident radiation between antennas to be given by $\phi=kd\sin(\theta)$, the electrical angle [13]. It is also possible to use two dimensional arrays which would of course allow cancellation of interference in two dimensions. We assume that the direction of the interference is unknown, but is stationary over the convergence time of the adaptation

algorithm. Also, it is assumed that variance (power) of the interference is greater than the signal(s) of

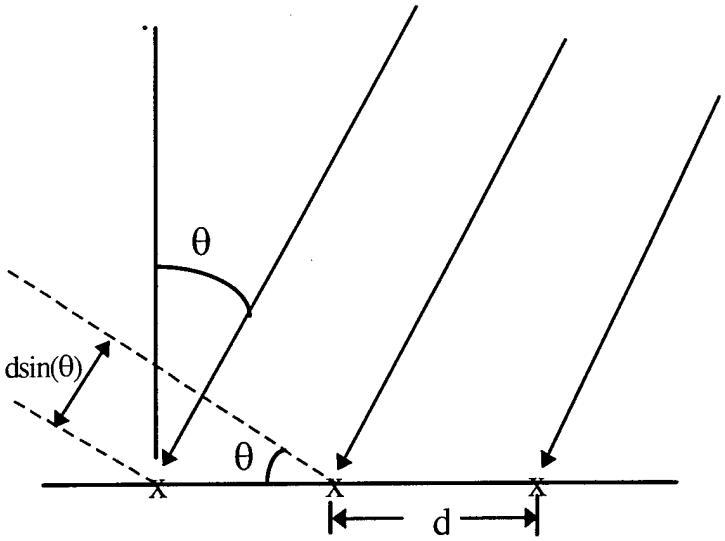

Figure 5.1: Geometry of adaptive beamforming array

interest. This means that if we let the signal vector be defined as $\mathbf{x}(t) = [x_1(t), x_2(t), \ldots, x_{n-1}(t)]^T$ then we should be able to attenuate the interference by minimizing the variance of

$$e(t) = x_0(t) - \mathbf{w}^H(t)\mathbf{x}(t) \qquad (5.1)$$

where $\mathbf{w}^T(t) = [w_1(t), w_2(t), \ldots, w_{n-1}(t)]$ is a set of weights which can slowly vary in time, $x_0(t)$ is viewed as the desired response, and e(t) can be viewed as the error signal. Traditional adaptive beamforming also places a constraint on the weight vectors to preserve a unity gain in a predetermined look direction. However, this also requires a minimum of three receivers to implement. Hence, we will concern ourselves only with minimizing modulus square of e(t).

In general, there are two traditional approaches of approaching the minimization problem. The first is to view the squared error $|e(t)|^2$ as a multivariate

function of the adaptive filter's weights. The instantaneous gradient can be formed which is then used to update the filter weights so that they follow the path of steepest descent. This is the reason the oldest version of the algorithm is called the method of steepest descent [13]. We will use a more widely used algorithm which is recursive and is easy to use called the least mean squares algorithm (LMS). The second general approach to this problem is to recognize that this problem is the same as a linear least squares problem. This can be implemented using algorithms such as recursive least squares, QR-decomposition, ect [13]. However, these algorithms are more computationally complex and are harder to implement than LMS.. The reason the recursive least squares and QR-decomposition algorithms exist is because they offer better convergence, but it was found the normalized LMS algorithm (a close variant to LMS) was sufficiently convergent for this problem. For these reasons, and because the experimental data that will be used only comes from two antennas we chose only to examine the LMS algorithm and its close relative the normalized LMS algorithm

The complete derivation of the complex LMS algorithm is given in Haykin where it is shown that it results in three basic steps [13]:

1) Filter output: $g(t) = \hat{\mathbf{w}}^H(t)\mathbf{x}(t)$

2) Estimation error: $e(t) = x_0(t) - g(t)$

3) Tap-weight adaptation: $\hat{\mathbf{w}}(t+1) = \hat{\mathbf{w}}(t) + \mu\mathbf{x}(t)e^*(t)$

This is simple to program especially in the case of two antennas because in that case the vectors reduce to scalars. The quantity μ is the step-size parameter, and determines the convergence properties of the LMS algorithm. Picking a value of μ which is to large will cause the algorithm to diverge and picking a value which is to small will make the adaptation time to long to be useful. It was found through trial and error that using this form of the algorithm on the set of radio broadcasts that were sampled did not yield useful convergence properties. However, if we modify the LMS algorithm by

normalizing the step-size parameter by the squared magnitude of the data vector, **x**(t), then the algorithm satisfactorily converged. Thus, the normalized least mean squares algorithm that was actually implemented in the following analysis modifies step 3 by [13]:

$$3)\quad \hat{\mathbf{w}}(t+1) = \hat{\mathbf{w}}(t) + \frac{\tilde{\mu}}{\|\mathbf{x}(t)\|^2 + k}\mathbf{x}(t)e^*(t)$$

where $\tilde{\mu}$ is the normalized step size and k is constant which insures that the denominator cannot become to close to zero. The values of $\tilde{\mu}$ and k that were used were 1 and 100, respectively.

In contrast to most adaptive filtering problems, the result that we want is not the filter output. Instead it is the error sequence that is of interest. The filter adjusts its tap weights so that its output closely models the main components of $x_0(t)$ which should be the direct signal and any strong clutter sources. Subtracting the two should leave scattered signals which arrived from different directions than the direct signal. This is of course the error sequence of equation 5.1, and is where we will start the analysis of how adaptive beamforming will affect the sensitivity of the FM radar.

5.2 ANALYSIS OF ADAPTIVE BEAMFORMING EFFECTS ON SENSITIVITY

To analyze the effects that adaptive beamforming has on the sensitivity of the FM radar system we limit ourselves to the simple case of two receivers. We do this because the direct signal is the major source of "interference" in this problem and because it should be easy to generalize from this example to more than two receivers. Also, the currently available experimental data was for only two receivers.

First, we write the two signals without including the noise terms because we will assume the clutter, direct, and scattered signal are all much greater than the noise. From chapter 2, we have:

$$x_0(t) = u(t) + \int_{R_d}^{\infty} \Phi_1(r,t)u(t-r)dr$$
$$x_1(t) = e^{j\phi}u(t) + \int_{R_d}^{\infty} \Phi_2(r,t)u(t-r)dr \tag{5.2}$$

where ϕ is the electrical angle, and Φ_1(t,r) and Φ_2(t,r) are the scattering amplitudes of the clutter and targets which are different because of the phase shift which is presumed unknown but different from the direct signal. If u(t) is significantly larger than the clutter, then we can assume the single spatial weight should converge to approximately $e^{j\phi}$, but there will be some error, ε. This means the resulting error term e(t) which now we will call y(t) is given as:

$$y(t) = \varepsilon u(t) + \int_{R_d}^{\infty} u(t-r)[\Phi_1(r,t) - e^{-j\phi}\Phi_2(r,t)]dr \tag{5.3}$$

Next, we form the product $y(t)x^*(t-r_0)$ as is done in the previous chapter's analysis. This results in:

$$y(t)x^*(t-r_0) = \varepsilon u(t)u^*(t-r_0) + \varepsilon \int_{R_d}^{\infty} \Phi_1^*(r'-r_0,t)u(t)u^*(t-r'-r_0)dr' +$$
$$\int_{R_d}^{\infty} u^*(t-r_0)u(t-r)[\Phi_1(r,t) - e^{-j\varphi}\Phi_2(r,t)]dr + \tag{5.4}$$
$$\int_{R_d}^{\infty}\int_{R_d}^{\infty} u(t-r)u^*(t-r'-r_0)\Phi_1^*(r'-r_0,t)[\Phi_1(r,t) - e^{-j\phi}\Phi_2(r,t)]dr$$

This can now be compared to the sequence a(t) as defined in the previous chapter. Notice that if we assume $|\varepsilon|<<1$, then the dominant terms in the sequence are:

$$y(t)x^*(t-r_0) \approx \int_{R_d}^{\infty} u^*(t-r_0)u(t-r)[\Phi_1(r,t) - e^{-j\phi}\Phi_2(r,t)]dr + \int_{R_d}^{\infty}\int_{R_d}^{\infty} u(t-r)u^*(t-r'-r_0)\Phi_1^*(r'-r_0,t)[\Phi_1(r,t) - e^{-j\phi}\Phi_2(r,t)]dr \tag{5.4}$$

This obviously shows that the clutter contribution due to the direct signal with itself is dramatically reduced if ε is small. Instead, now the important contribution to the variance of the probability distributions is the physical clutter. This shows that in the case of near ideal adaptive beamforming that the FM radar will be limited by the physical clutter in the environment. Also, since the target(s) of interest is implicitly included in the scattering amplitude, we see that another effect is that it can reduce the scattering amplitude of the target of interest by:

$$\alpha(1 - e^{j(\phi_T - \varphi)}) = \kappa\alpha \tag{5.5}$$

where ϕ_T is the electrical angle of the target of interest and ϕ is the electrical angle corresponding to the direct broadcast. The value of κ can be between 0 and 2. This also occurs for any physical clutter in the problem and shows that adaptive beamforming could actually increase the contribution to the variance by some of the physical clutter.

Now we use the factor ξ from before to represent the ratio of the physical clutter to the broadcast signal's power as given by:

$$\xi = std[\mathrm{Re}\{y(t)x^*(t-r_0)\}] / \sqrt{2}\sigma_t^2$$
$$\sqrt{2}\sigma_t^2 = std[\mathrm{Re}\{x(t)x^*(t-r_0)\}] \tag{5.6}$$

then we may write the variance of the unnormalized chi-square as:

$$\sigma_S^2 = \frac{2\xi^2\sigma_t^4 N}{MS} + \gamma = \frac{2\xi^2\sigma_t^4 N}{MS}\left(1 + \frac{MS\gamma}{2\rho^2\sigma^4 N}\right) = \frac{2\xi^2\sigma_t^4 N}{MS\beta} \tag{5.7}$$

Then we can rewrite the noncentrality parameter as:

$$\lambda = \Omega / \sigma_S^2 = 2\kappa^2 \alpha^2 T\beta / \xi^2 \tag{5.8}$$

where κ is the loss factor due to the distortion of the beam in the direction of the target, ξ is the gain due to cancellation of the direct signal, and β is the loss factor as defined before. This means we can rewrite equation 4.46 for the case of adaptive beamforming as:

$$\text{M>2} \qquad \alpha_{\min}^2 = \frac{1 + 3.464n\sqrt{M} + 2.828k\sqrt{M} + 1.5n^2 + 2.449nk + k^2}{2T\beta\kappa^2}\xi^2 \tag{5.9}$$

Notice that if $\xi/\kappa < 1$ for most electrical angles then adaptive beamforming should be useful barring a dramatic change in β.

5.3 EXPERIMENTAL RESULTS

The previous section showed that the key to understanding the improvement offered by adaptive beamforming or directional antennas is the characterization of the typical physical clutter. The best way to do this is simply to turn on the receivers and make measurements of the clutter environment using adaptive beamforming. It should then be possible to estimate ξ.

Estimating ξ requires that we first find the standard deviation of the direct signal plus the physical clutter and then use adaptive beamforming to estimate the standard deviation of the physical clutter only. This results in the following estimate:

$$\frac{(1+\hat{\xi})\sigma_{direct}}{\hat{\xi}\sigma_{direct}} = \frac{\sigma_{scatt+direct}}{\sigma_{scatt}} = k \Rightarrow \hat{\xi} = \frac{1}{k-1} \tag{5.9}$$

where σ_{direct} is the standard deviation of the $u(t)u^*(t-r_0)$ where $u(t)$ is the direct signal.

Only one set of data was available to determine whether adaptive beamforming improves the sensitivity of the radar. The results were encouraging. The data is signal A2 and a new data set B2 which was synchronously sampled by a different receiver. The baseline was 1.5 meters. After the data was passed through the adaptive beamforming algorithm the standard deviation of the real and imaginary parts were computed. It was found that they were both approximately 10. In contrast, signal A which was used as the reference signal had a standard deviation that for both in-phase and quadrature was 30. This gives a ratio of 1/3. This meant that ξ should be 1/9. However, a calculation of ξ for r_0 = 21 km showed that it remained about 1/3. This indicates that the contribution of the physical clutter to the standard deviation is more than is predicted and probably occurs because of more correlation due to physical clutter.

However, ξ being close to 1/3 shows that some improvement is possible. Notice that this means it could improve the sensitivity by a factor of 1/9 which is about 9.5 dB. To test this we injected the same target into both A2 and B2 that was used in figure 4.28. Figure 5.1 shows that it is plainly distinguishable. Figure 5.2 shows a target 3.3 dB below the one used in figure 5.1. Notice it is still visible. This seems to indicate at least a 6 dB gain in this case. It was also known that the signals used were quite noisy. With better receivers it may be possible to improve the gain of the adaptive beamforming system.

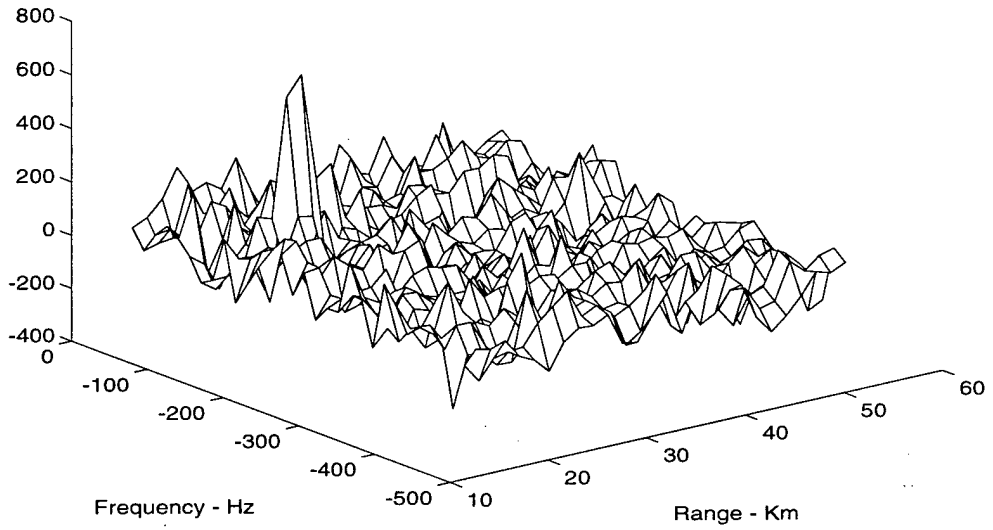

Figure 5.2: Plot of |X(r,-f)| - |X(r,f)| for the cross ambiguity plot of the adaptive beamformed signal with A2. Λ_s =128,000, M = 8, and the amplitude level the same as 4.30.

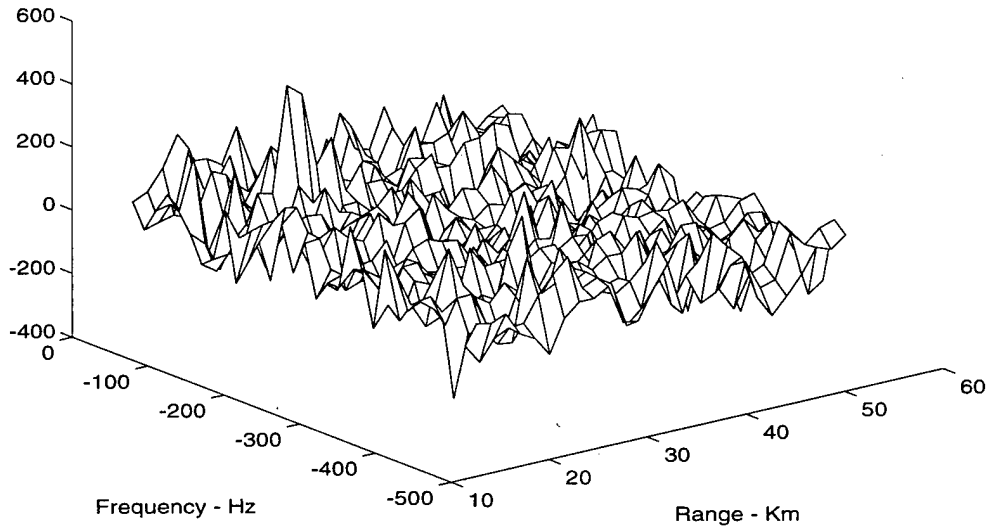

Figure 5.3: Plot of |X(r,-f)| - |X(r,f)| with the same parameters as figure 5.2 except the scattering amplitude is 3.3 dB less.

CHAPTER 6: RESULTS AND CONCLUSION

Throughout this thesis we have been exploring the sensitivity of the monostatic FM radar. The key issue in determining the sensitivity is the ratio of the scattered signal to the direct signal. The introduction shows that to be useful the bistatic system must be able to detect signals whose SDR are less than -54 dB. Unfortunately, because the bandwidth of the FM broadcasts is insufficient it is probably not possible to us FM radio broadcasts to detect aircraft. However, if control of the transmitting waveform is possible then a white Gaussian noise signal with sufficient bandwidth should be possible.

6.1 WHITE GAUSSIAN SIGNAL RADAR NETWORKS

Equation 4.35 which determines the minimum SDR shows the strong dependence of sensitivity on bandwidth. Throughout the thesis we have constrained ourselves to processes with bandwidths on the order of 250 kHz. Notice that if the bandwidth is increased to 10 - 20 Mhz, the radar now becomes sensitive to targets with SDRs in the range of -60 dB. Because of the wide bandwidth of these signals, it is probably desirable to move the carrier frequency into the 3 - 10 Ghz range so that the narrowband scattering approximation still applies. However, it obvious there are two problems that are encountered with the practical implementation of the above system. The first is the increase of noise power with bandwidth, and the second is the increase in computational burden as the bandwidth increases.

First, we examine the increase of noise power with bandwidth. If we increase the carrier frequency to 3 - 10 Ghz, then the noise floor can be approximated by the cosmic background radiation if we use good receiver design [14]. This means that equation 1.4 can be use to approximate the noise floor with T being approximately 5 K. This means that with a 10 Mhz system that the total noise power is only 6.9×10^{-16} Watts

which is still far below the signal power at distances of interest. In fact, increasing bandwidth will result in gain versus noise because from equation 4.46 the increase in gain is linear with a slope of approximately one. In contrast, the noise power increases linearly with bandwidth but with a slope of $N_0 = 6.9\times10^{-23}$ W/Hz. The way to think about what is occurring is to realize that by increasing the bandwidth of the signal its power is being spread in frequency because we are forcing it to be white. However, the scattered signal's energy still remains the same. From this it follows that as the bandwidth is increased the system will eventually reach the point of being the noise limited matched filter output with SNR given by:

$$\frac{2E_s}{N_0} \tag{6.1}$$

Where E_s is the energy content of the scattered signal for the integration time. Notice that N_0 is not dependent on bandwidth, and therefore determines the ultimate sensitivity of the radar system for a fixed transmitter power.

The second problem is the issue of computation of the ambiguity function for bandwidths of 10 - 20 Mhz. The computation requirement of the ambiguity function can basically be broken down into two steps. First, we perform coherent integration to reduce the bandwidth of the signal. The bandwidth of the targets of interest depend on the carrier frequency and the maximum radial velocity they obtain. For man-made objects, we can take the maximum radial velocity as about 1000 m/s. This means that at a carrier frequency of 3 Ghz we can expect a maximum doppler shift of 63 kHz. This means our complex sampling frequency should be 63 kHz. Hence, if we are operating with a bandwidth of $2^{24} \approx 16.78$ Mhz then we can decimate by a factor of D = 256. We must do that for each range of interest with 225 ranges required if we wish to use the maximum range resolution for 0 to 4 km. Following this, each range must be fourier transformed to give the frequency spectrum of the scattering amplitudes. This means it requires 4.01×10^9 complex multiplies per second which since each complex multiply requires four real

multiplications translates into 16×10^9 real multiplications. The general expression for algorithms with $f_B/D = 2^n$ where n is an integer is given for multiplications as:

$$f_B R(1+\frac{\log_2(f_B / D)}{D}) \tag{6.2}$$

where R is the number of ranges to examine. Notice that the decimation step, $f_B R$, dominates if D is even moderately large. Thus, although the operations count is at first apparently daunting it should be possible because of the simplicity of the decimation step to effectively implement the algorithm in most cases.

6.2 CONCLUSION

The investigation of the possibility of using FM radio broadcasts in a monostatic version of the radar was shown to be ineffective primarily because the bandwidth of the FM broadcast was not wide enough to give sufficient signal processing gain to detect point targets such as aircraft. However, the results of the investigation have shown that monostatic radars which use wide bandwidth white gaussian signals approach the maximum SNR available from a signal processed by a matched filter in the background of the cosmic noise floor. This shows promise in developing passive radar networks and even passive radars which would be capable of operating without detection. It has also been shown how to determine the probability density functions of the ambiguity function which is used to detect targets. This is important because it allows the performance of the radar to be determined as a function of the false alarm probability and detection probabilities.

As with any complex problem, there is still much that remains to be explored. The power of the physical clutter relative to the direct signal has not been adequately estimated. The geographic location of the transmitters and receivers with relation to the target of interest can also have a profound effect on the radar's performance. An analytical model of the effect of the noise being colored instead of

white could also give much insight. Finally, an actual experiment using wide-bandwidth white gaussian signals could be conducted.

List of References

[1] Personnel Correspondence with Frank Lind a Ph.D. candidate in the Department of Geophysics at the University of Washington who was currently building the radar receivers at the time this report was prepared, August 1996 - September 1997.

[2] Whalen A. D., McDonough R. N., *Detection of Signals in Noise*, 2nd ed., Academic Press, San Diego, 1995.

[3] Skolnik, M.I., *Introduction to Radar Systems,* 2nd ed., McGraw-Hill, New York 1990.

[4] Hall, P. W. "Correlative Range-Doppler Detectors and Estimators in Bistatic Radar using Commercial FM Broadcasts," Masters Thesis, Dept. Electrical Engineering, University of Washington, Seattle, WA, 1995.

[5] Ishimaru, A., *Electromagnetic Wave Propagation, Radiation, and Scattering*, Prentice Hall, New Jersey, 1991.

[6] Hansen, J. M., "A New Radar Technique for Remote Sensing of Atmospheric Irregularities by Passive Observation of the Scattering of Commercial FM Broadcasts," Masters Thesis, Dept. Electrical Engineering, University of Washington, Seattle, WA, 1994.

[7] Ishimaru, A., *Wave Propagation and Scattering in Random Media*, IEEE Press, New York, 1997.

[8] Levanon, N., *Radar Principles*, John Wiley & Sons, New York, 1988.

[9] Percival D. B., Walden A. T., *Spectral Analysis for Physical Applications*, Cambridge University Press, New York, 1993.

[10] Papoulis, A., *Probability, Random Variables, and Stochastic Processes*, McGraw-Hill, New York, 1991.

[11] Lind F. D., Sahr J. D., "The Manastash Ridge Radar: A Passive Bistatic Radar for Upper Atmospheric Radio Science," Accepted for publication in Radio Science, 1997.

[12] Abramowitz M., and I. A. Stegun, eds., *Handbook of Mathematical Functions*, Applied Mathematics Series-55 (AMS-55). Washington, DC: National Bureau of Standards (1964). Paperback edition, New York: Dover (1964).

[13] Haykin, Simon S., *Adaptive Filter Theory*, Prentice-Hall, New Jersey, 1986.

[14] Hagen, Jon B., *Radio Frequency Electronics: Circuits and Applications*, Cambridge University Press, 1996.